












RESEARCH ARTICLE

WILEY

Bofedal wetland and glacial melt contributions to dry season streamflow in a high-Andean headwater watershed

Tom Gribbin^{1,2}  | Jonathan D. Mackay^{1,2}  | Alan MacDonald³  |
 David M. Hannah²  | Wouter Buytaert⁴  | Jan R. Baiker⁵  |
 Nilton Montoya⁶  | L. Baker Perry⁷  | Anton Seimon⁷  | Maxwell Rado⁶  |
 Sandro Arias⁸  | Miguel Vargas⁶

¹British Geological Survey, Environmental Science Centre, Keyworth, UK

²School of Geography, Earth and Environmental Sciences, University of Birmingham, Edgbaston, UK

³British Geological Survey, The Lyell Centre, Edinburgh, UK

⁴Civil and Environmental Engineering, Imperial College London, London, UK

⁵Asociación para la Conservación y Estudio de Montañas Andinas-Amazónicas (ACEMAA), Cusco, Peru

⁶Departamento Académico de Agricultura, Universidad Nacional de San Antonio Abad del Cusco (UNSAAC), Cusco, Peru

⁷Department of Geography and Planning, Appalachian State University, Boone, North Carolina, USA

⁸National Service of Meteorology and Hydrology of Peru/SENAMHI, Lima, Peru

Correspondence

Tom Gribbin, British Geological Survey, Environmental Science Centre, Keyworth NG12 5GG, UK.

Email: tgrib1@bgs.ac.uk

Funding information

Natural Environment Research Council, Grant/Award Numbers: NE/S013210/1, NE/X006255/1, NE/S007350/1, NEIF#2573; Consorcio para el Desarrollo Sostenible de la Ecorregión Andina (CONDESAN)

Abstract

In the context of expected future melt reductions in the high-Andes, the buffering capacity of non-glacial stores, and especially of high-altitude bofedal wetlands, is of increasing importance. Isotope signatures potentially indicative of water undergoing evaporation on transit through bofedales have been found in the tropics, but end-member uncertainty has so far prevented streamflow separation using this signal. We undertook a stable isotope sampling campaign over the 2022 wet-dry season transition in a 53.6 km², 16% glacierized catchment in southern Peru with a bofedal coverage of 11%. Diurnal proglacial hydrographs and remote sensing were used to interpret seasonal snowmelt dynamics and identify the dry periods when glacial melt and bofedal contributions are assessed to be the two principal components of streamflow. Following the final wet season precipitation event, a rapid ~3 week transition occurs in the main river from a stable isotope signature consistent with dynamic rainfall/snowmelt contributions to one of ice-melt. In both wet and dry seasons, the main river and tributary streams show evaporative enrichment suggesting ongoing supply from water transiting bofedales. A two-component mixing model using $\delta^{18}O$ -excess during the dry season shows the bofedal source contribution varies from 9% to 20% [± 9 –10%], indicating that streamflow is greatly augmented by the presence of glaciers at these headwater scales. However, applying these proportions to river discharge shows a sustained bofedal contribution of around 0.09 m³/s during the dry season study window whereas the flux of glacial water halves from 0.73 to 0.36 m³/s over this timeframe. The results highlight the important role of bofedales and the connected groundwater system in buffering seasonal declines in streamflow months into the dry season, and suggests the hydrological functioning of bofedales as part of this wider system should be considered when exploring the effectiveness of potential options to sustain baseflows in a post-glacial future.

This is an open access article under the terms of the [Creative Commons Attribution](https://creativecommons.org/licenses/by/4.0/) License, which permits use, distribution and reproduction in any medium, provided the original work is properly cited.

© 2024 British Geological Survey (C) UKRI and The Author(s). Hydrological Processes © 2024 John Wiley & Sons Ltd.

KEYWORDS

bofedales, high-altitude wetlands, isotope hydrology, Quisoquipina, tracer hydrograph separation, Vilcanota

1 | INTRODUCTION

Mountains are the world's water towers, generating disproportionately high runoff from precipitation compared with their spatial extent, and releasing water to downstream populations (Immerzeel et al., 2020; Viviroli et al., 2007; Viviroli et al., 2020). The cryosphere is an important moderator of stream regimes in many mountain headwaters, with glacier and snow melt sustaining streamflow during drier months of the year (Fountain & Tangborn, 1985; van Tiel et al., 2020). In the Andes, tropical glaciers are particularly sensitive to climatic changes and are undergoing rapid rates of recession (Dussaillant et al., 2019; Salzmann et al., 2013; Taylor et al., 2022; Vuille et al., 2018), increasing the exposure of downstream populations to issues of water supply especially during drought years. In the affected headwaters, high-mountain communities with lower adaptive capacity are some of the most at risk from climate-induced glacier change (Buytaert et al., 2017; Drenkhan et al., 2023; Postigo, 2021).

However, even at close proximity to glaciers where melt contributions are most significant, streamflow variability is also buffered to some extent by the storage and release dynamics of other stores, such as surficial and bedrock aquifers, lakes and wetlands (e.g., Chesnokova et al., 2020; Drenkhan et al., 2023; Glas et al., 2018). Quaternary deposits from current and previous glaciations can provide the conditions necessary for the development of strategically important aquifers with high permeability and storage capacity (Ó Dochartaigh, MacDonald et al., 2019; Emmer, 2024) and for the formation of expansive wetlands in wide glaciated valley bottoms (Hayashi, 2020; Somers & McKenzie, 2020). The structure of coarse talus and solifluction deposits at the hillslope-valley interface is an important control on the connectivity of high-elevation source areas to underlying groundwater units (Baraer et al., 2015; Glas et al., 2019; Ó Dochartaigh, Archer et al., 2019). Further, moraine and slope deposits can provide ongoing supply to higher order streams months after the cessation of rainfall (Caballero et al., 2002; Gordon et al., 2015; Muir et al., 2011). Representation of these source contributions is increasingly important as the glacial meltwater component declines and other water sources form a greater proportion of streamflow (Somers et al., 2019).

The hydrological functioning of peat-forming high-altitude wetlands (known locally as 'bofedales') has become an important focus of research in the puna ecoregion of the southern tropical Andes. The distinct hydrophytic plant assemblages that constitute bofedales develop in depressions and along small springs and streams and are supplied by melt water, groundwater and precipitation (e.g., Cooper et al., 2010; Maldonado Fonkén, 2014). Bofedales are important sites for carbon sequestration (Hribljan et al., 2015), livestock grazing (Yager et al., 2019), and endemic species (Oyague & Cooper, 2020), as well as potentially sustaining baseflows during the protracted dry

season (Ross et al., 2023; Wunderlich et al., 2023). Baseflows may be sustained by the hydrophysical properties of the bofedal soils themselves (Buytaert et al., 2011; Rezanezhad et al., 2016), by changes in bofedal network connectivity as water levels rise and fall seasonally (Buytaert & Beven, 2011) and even by the densely packed structure of bofedal plant shoots at the surface (Oyague & Cooper, 2020). Importantly, as post-glacial features, bofedales are often found in low gradient valley-bottom areas fed by large contributions of upslope groundwater (Cooper et al., 2019; Wunderlich et al., 2023), with various post-glacial storage units such as moraine (e.g., Gordon et al., 2015), talus (e.g., McClymont et al., 2010) and sandurs (e.g., MacDonald et al., 2016) potentially interacting with bofedal waters.

The high variability of the input and output fluxes to bofedales makes disentangling the overall contribution to streamflow extremely difficult using hydrometric methods. Across three extensively instrumented sites in central Peru, Oyague et al. (2022) found highly localized bofedal water table dynamics despite similar seasonal precipitation regimes, peat thicknesses and landscape positions. Similarly, Ross et al. (2023) observed large intra-site differences in water table response in the upper Vilcanota-Urubamba basin (VUB). The authors used these responses to partition different subsurface components of streamflow using a novel unit-hydrograph modelling approach, but disaggregation of the bofedal from the hillslope component ultimately remained elusive without more observational data. The challenge of using a hydrometric approach was further exacerbated by the additional melt term in the glacierized study catchment, and the authors had to make use of a modelled multiyear mean melt flux despite the potential interannual variability. Even where spatio-temporal bofedal water table dynamics have been constrained and evaporation accounted for (e.g., the study of Wunderlich et al. (2023) in an unglacierized catchment also in the VUB), dry-season bofedal water storage reductions do not necessarily translate to equivalent streamflow contributions at the catchment scale due to potential recharge of deeper groundwater stores which bypass the gauge at the spatiotemporal scale of study. In glacierized catchments, potential melt inputs to bofedales must also be considered (directly via melt stream networks or indirectly via groundwater recharge) although studies have drawn differing conclusions about the significance of such interactions (Cooper et al., 2019; Dangles et al., 2017; Polk et al., 2017).

Given the challenges of using water balance methods for hydrograph separation in catchments with extensive bofedal coverage, stable isotopes provide a promising alternative approach. Stable isotopes of water are conservative tracers in the typical temperatures of the subsurface, but undergo fractionation during evaporation (Gat, 2010). This behaviour allows evaporating sources to be separated from other source contributions using a dual isotope framework, and has been widely applied to quantify lake and wetland contributions to

streamflow in studies worldwide (e.g., Brooks et al., 2018; Burns & McDonnell, 1998; Gibson & Reid, 2010; St Amour et al., 2005), though not yet in high-Andean catchments. Previous hydrogeological studies in the Cordillera Blanca (CB) in Peru have used both isotopic and geochemical approaches to understand the interactions and relative contributions of groundwater and glacial melt, but clear evidence of fractionation has been found only in proglacial lakes rather than in valley-bottom meadows, and isotopic data has largely been used only to infer originating source elevations rather than to separate the contributions of intermediate stores (Baraer et al., 2015; Gordon et al., 2015). However, there are reasons to suggest that the 'evaporative fingerprint' of water transiting bofedales may yet be identified in other Andean headwaters.

First, the steep valleys of the CB have only relatively small proportions covered by saturated bofedales. In two CB study sites described as indicative of other valleys Gordon et al. (2015) classify only 1.5% and 3% of the total area as meadow (in the study 'meadow' is equated with 'bofedal'). Meadow areas are further subdivided into 'wet meadows' or 'valley-fill grassland', highlighting that even where bofedales have been identified the water table is potentially at some distance below the surface and not necessarily exposed to evaporation. Synoptic sampling efforts have also focussed either on sampling springs directly at source where the water will have had little time to undergo evaporation in any bofedal surface stream networks that do occur, or on sampling groundwater wells that penetrate the upper organic and clay bofedal layers and are screened in the sand or gravel units beneath.

Second, an evaporative isotopic signal has been previously observed in streamflow at both catchment and regional scales (Hill et al., 2018; Williams et al., 2001), but has not been definitively linked to the contributing source. Williams et al. (2001) found an enrichment in $\delta^{18}\text{O}$ of about 4% within 7 km of a glacier tongue in the Ecuadorian high-altitude grasslands but could not determine whether the enrichment was due to mixing with isotopically enriched rain, evaporation in bofedales, or some combination of the two. Hill et al. (2018) undertook basin-wide synoptic sampling of surface waters from high to low elevation in the CB and observed a similar signal in the headwaters that was absent in low-elevation jungle or transition zones. Cooper et al. (2019) sampled two high-altitude river reaches flanked by peatlands in Bolivia, suggesting that the more positive $\delta^{18}\text{O}$ values of peatland and stream waters relative to hillslope springs was indicative of evaporative enrichment between the hillslopes and the stream. In these studies, the dearth of isotope measurements of precipitation in the tropics generally (Sánchez-Murillo et al., 2019; Terzer-Wassmuth et al., 2020) and in the southern Peruvian Andes specifically (Valdivielso et al., 2020), presented significant challenges to identifying whether precipitation dynamics or in-catchment processes were driving the isotopic signal in streamflow.

In our study we undertake synoptic sampling across a glacierized headwater catchment with high bofedal coverage (11%), in a region where excellent baseline isotopic precipitation data is available (Guy et al., 2019). We aim to understand the spatio-temporal dynamics of groundwater, bofedal and glacial contributions to streamflow. Our specific research objectives are: (1) to identify the water source dynamics and processes that explain the longitudinal and temporal

isotopic evolution in streamwater; and, (2) to quantify the contribution of water transiting bofedales to streamflow for all appropriate periods during the dry season.

2 | STUDY AREA

Peru contains 68% of the world's tropical glaciers, though 56% of the original glacier area has been lost between 1962 and 2020 (INAIGEM, 2023). The SQC (equivalent to the Ross et al. (2023) study catchment) is a 54.1 km², 16% glacierized catchment located in the headwaters of the Vilcanota River, part of the high-plateau Antiplano region in the Eastern Cordillera of Southern Peru (Figure 1). The Cordillera Vilcanota is the second largest tropical glacierized mountain range in the world (after the CB), and includes the world's largest tropical glacier, Quelccaya, 10 km SW of the SQC. Ice core records extracted from Quelccaya since the early 1980s (Thompson et al., 1985) give an annually resolved palaeoclimate record for the last 1500 years, and have provided the impetus for modern-day collection of precipitation isotopes to understand meteorological controls on spatiotemporal variability (Guy et al., 2019).

The SQC is orientated NE-SW with an elevation range from 4746 to 5770 m asl. At the head of the 12 km main valley, the Quisoquipina and Suyuparina glaciers cover 5.78 km² and make up 67% of the glacial area (Figure 1a). Two tributary valleys, approximately half-way down the catchment, mark the approximate lower limit of the glacial coverage. The bedrock geology is predominantly the Mitu Formation, a complex succession of sedimentary lower units and andesitic and basaltic lavas in the upper units (Soberon et al., 2022). The fine-medium grained sandstones of the Ambo Group underlie the Mitu Formation, and outcrop up-valley in the SQC closer to Quisoquipina. Superficial glacio-fluvial deposits including Holocene moraine complexes and peat deposits extend over the valley-bottoms. Our observations in the SQC and studies nearby (King et al., 2021; Perez & Loisel, 2023) indicate typical peat depths of 0.5–1.5 m overlying clay-rich mineral layers interspersed with further peat phases down to depths of >5 m. The saturation area varies seasonally, and our field observations suggest that the satellite derived bofedal extents in Figure 1b are a good proxy for water tables within about a metre of the surface. Stream networks meander through the peatland connecting pools in the bofedal forming a distributed network (Figure S1d–g). We assume flow through the peat is generally consistent with the surface topography (Bertassello et al., 2020), which slopes toward the river and down-valley at roughly 45° to the river in the largest bofedales in the main valley (L1 and L2, Figure 1b, Figure S2). In some places, anthropogenic channels contour from the main river across the surface topography to further irrigate sections of the bofedal directly from the river (Figure S1b), although topographic constraints limit such surface supply to areas close to the main river (<100 m).

Precipitation is driven largely by advective moisture transport from the nearby Amazon basin (Drenkhan et al., 2019; Perry et al., 2017), and is highly seasonal, with 85%–94% of total annual

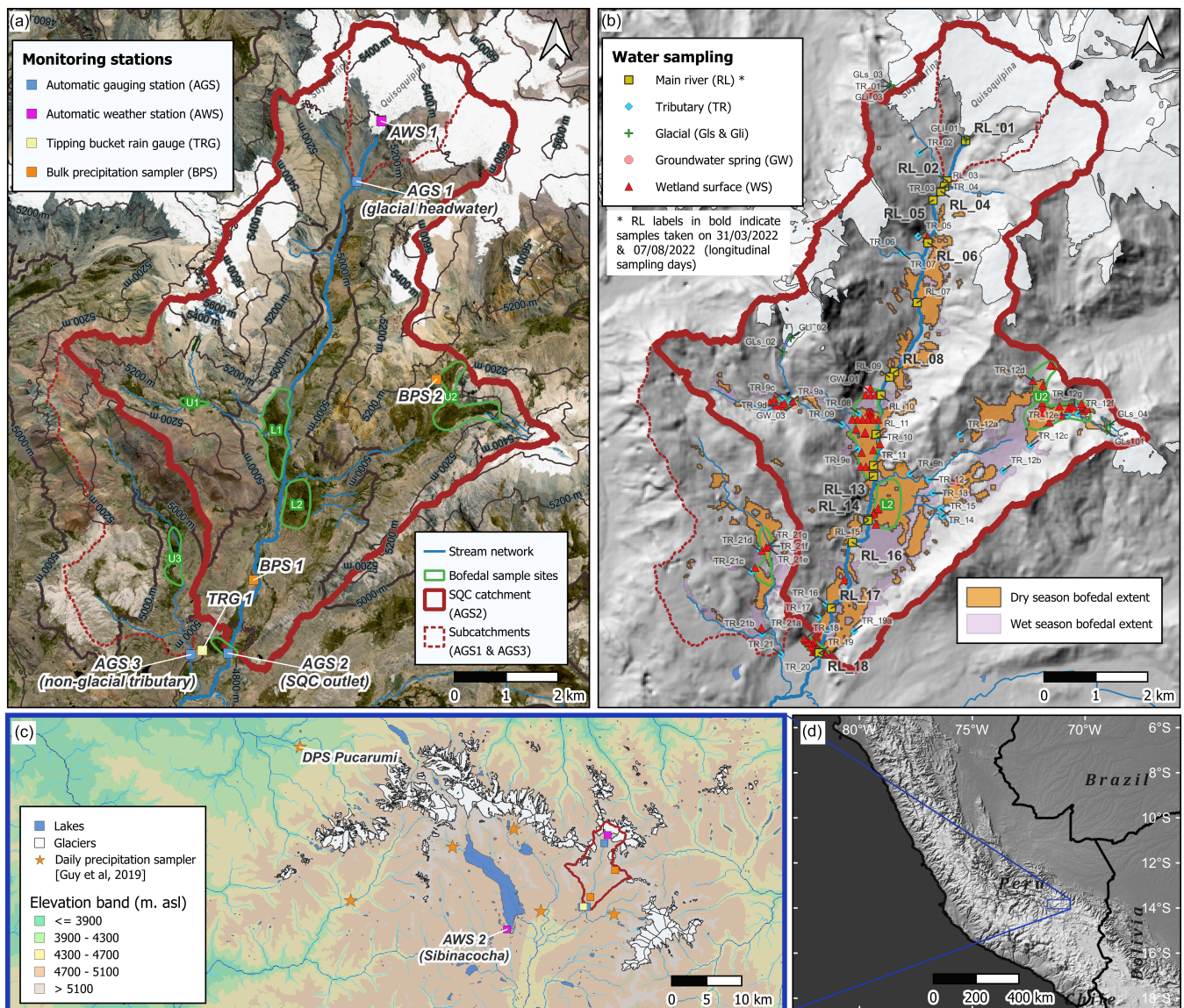


FIGURE 1 (a) The Suyuparina Quisoquipina catchment (SQC) and hydrometeorological monitoring stations used in the present study. Bing satellite basemap (acquisition date 30/06/2016) and field observations used to manually map stream network. (b) Water sample locations by sample type. Glacier and lake extent from 2020 inventory of (INAIGEM, 2023). Bofedal extents show remote sensing derived bofedal extents at the end of the 2020 dry season and end of the 2021 wet season (Ross et al., 2023). Hillshade basemap generated from ALOS satellite (JAXA, 2021). (c) Regional monitoring station locations with respect to the SQC. Elevation bands derived from SRTM satellite (NASA JPL, 2013), glacier and lake extent from 2020 inventory of (INAIGEM, 2023) and regional stream network from Amatulli et al. (2022) global hydrography dataset (only strahler stream orders >2 shown). d) SQC location within Eastern Cordillera of Southern Peru.

precipitation (666–954 mm) recorded at Sibinacocha AWS falling during the austral summer ‘wet season’ months of October–March (Table S1).

Precipitation phase within the SQC is strongly related to elevation. Above 5000 m asl solid precipitation dominates at over 95% of precipitation hours, but the solid–liquid transition is only a few hundred metres lower. At the SQC valley floor elevation (4800 m asl) precipitation is likely to fall as rain approximately half of the time (Endries et al., 2018; Perry et al., 2017). Diurnal precipitation patterns exhibit a bimodal pattern, with mid-afternoon convective rainfall and nocturnal stratiform events associated with moisture sourced from deep moist

convection over the adjacent Amazon lowlands (Perry et al., 2014; Perry et al., 2017). At the scale of the Vilcanota basin, the north–south dominant precipitation trajectory results in a weak relationship of precipitation amount with elevation (Fyffe et al., 2021). At nearby Sibinacocha (4895 m asl) the seasonal range in mean daily temperature is small (JAS min = 1.5°C, JFM max = 2.7°C) compared to the much larger diurnal range. Seasonal mean diurnal minima are below freezing at night in all seasons (JAS min = −4.1°C, JFM max = −0.1°C) but mean diurnal maxima reach temperatures of between 6.9°C (JFM) and 8.0°C (JAS) in the afternoon (Figure S3), ensuring that the off-glacier snowpack is highly ephemeral in the SQC. On-glacier, monthly snow

depths are extremely shallow in Quisoquipina glacier ablation zone at AWS1, with continuous melting and reformation recorded over periods of days to weeks (Fyffe et al., 2021). Precipitation dynamics are a critical control on glacial mass balance as net shortwave radiation dominates, being primarily controlled by albedo and therefore by snowfall (Fyffe et al., 2021; Suarez et al., 2015).

3 | DATA AND METHODS

3.1 | Meteorological data

Hourly temperature, humidity and wind speed data were used from a tripod-on-ice automatic weather station installed at 5157 m asl on Quisoquipina Glacier (AWS1, Figure 1a). Precipitation amount is not monitored at AWS1 but a shielded Pluvio2 weighing precipitation gauge is located 16 km SW of the SQC at Sibinacocha dam (AWS2, Figure 1c). In December 2021, a HOBO tipping bucket rain gauge was installed in the SQC valley floor at 4800 m asl (TRG1, Figure 1a).

Guy et al. (2019) published baseline isotopic precipitation data collected by citizen scientists from 2013 to 2017 and derived local meteoric water lines (LMWLs) describing the $\delta^{18}\text{O}$ - $\delta^2\text{H}$ ratio in precipitation for sites across the region (Figure 1c). The Pucarumi citizen scientist continued collection from 22nd August 2019 to 23rd August 2023 and this updated dataset is presented to contextualize the results of the SQC sampling campaign.

3.2 | River stage data

River stage was measured by automatic gauging stations (AGS) at three locations in the SQC (Figure 1a). AGS1 is a pressure-transducer type (Solinst Levellogger 5) measuring stage every 30 min, installed in 2016 in a steel pipe fastened to a large boulder (Figure S1a) 1 km downstream of Quisoquipina Glacier. Landcover in the 5.05 km² AGS1 catchment is predominantly glacial (61%) with the remainder a mixture of freshly exposed subglacial sediment and bedrock (39%). Continuous measurements are available for 4 years from 2019 to 2022. Low flows at AGS1 in the dry months of June–August allowed nightly (9 pm–9 am) ice build-up around the steel pipe and caused a ‘spiking’ artefact in the apparent water level. For temporal consistency and comparability, observations between 9 pm–9 am were removed and daily stage calculated using the daytime observations only. AGS2 is the principal AGS in the SQC, and was installed in February 2022 under ‘Halairipampa bridge’ (Figure S1h), following a flood event which destroyed the previous monitoring station used in Ross et al. (2023). AGS3 was installed in March 2022 at ‘Viluyo bridge’ (Figure S1i), a non-glacierized tributary draining a catchment area of 10.65 km² with a confluence 500 m downstream of AGS2. AGS2 and AGS3 are fixed underneath the bridge structures monitoring distance to the water surface at intervals of 10–15 min, averaged to daily frequency. Eight manual flow gauging measurements were made between March 2022 and September 2023 to formulate a rating curve at AGS2.

3.3 | Snow cover

Snow cover maps were generated using Sentinel-2 satellite imagery to identify the dates when streamflow contributions from snowmelt are likely to be significant. The normalized-difference snow index (NDSI) is a simple method to identify snow cover from satellite imagery based on the principal that snow reflection is significantly higher in the visible spectrum than in the infrared (Härer et al., 2018). The 5-day revisit time and 20 m grid resolution of Sentinel-2 allows high-frequency characterization of snow and ice-cover, depending on cloud conditions at the time of acquisition. A cloud cover mask, NDSI, and visible bands were downloaded for all available imagery from 1st Jan to 31st December 2022 from the Sentinel Hub. A binary classification for snow/ice presence was calculated for each pixel within the catchment using a threshold NDSI of 0.42 (ESA, n.d.). Due to the occasional misclassification of cloud and snow pixels, a manual assessment of dates containing only completely clear sky conditions was made using the imagery from the visible spectrum, plotted alongside the cloud cover and NDSI masks (Figure S4). A Sentinel DEM acquired in June 2022 was used to bin the snow cover into 10 equal-area elevation bands.

3.4 | Water source sampling for stable isotopes and specific electrical conductance (SEC)

Wet (25th March–1st April 2022) and dry (6th August–18th August 2022) season sampling campaigns were undertaken across the SQC (Figure 1b). The same points on the main channel and principal tributaries were sampled in both campaigns to characterize the downstream non-glacial inputs. From 10th April to 26th June, 12 weekly samples were collected by a citizen scientist at AGS2 (equivalent to RL18 in Figure 1b) to supplement the campaign sampling.

Solid (Gli) and liquid (Gls) glacial samples were collected from two glacier margins (Gli_02, Gli_03), one proglacial lake outlet (Gls_02) and three proglacial streams (Gls_01, Gls_03, Gls_04) in the August 2022 campaign, but in the March 2022 campaign only from one glacier margin (Gli_01) due to possible mixing with dynamical snowmelt contributions in surface waters and difficulties accessing other sites. For the solid samples, ~1 kg of surface ice at the margin was removed and placed immediately inside three sealed ziplock bags and allowed to fully melt before transferring to HDPE bottles. A 60 cm deep snowpack sampled at 5157 m asl on the glacier margin (near GLs_03 in Figure 1b) in March 2022 allowed retrieval of 12 depth-dependent snow points captured at 5 cm intervals. Three well-defined refrozen ice lenses in the snowpack indicated accumulation-melt cycles from a number of precipitation events.

Bulk precipitation (PALMEX) samplers designed to prevent post-collection evaporation (Gröning et al., 2012) were installed from March 2022 to August 2022 (BPS1 (4780 m) and BPS2 (5112 m); Figure 1a) and captured the integrated signal over the wet-dry transition period.

Groundwater samples (GW) were collected at source from perennial springs, identifiable as those with flow in August 2022. Sampling

of springs at source prior to mixing in bofedales proved difficult. The mapped dry-season bofedal extent is strongly associated with areas where groundwater exfiltration is likely to occur (e.g., at the changes in slope at the valley margins; Figure S1f), and we observed in the field that the emergence of groundwater frequently occurred within the bofedal itself. The widespread interconnection with the bofedal system meant that definitive identification and sampling of groundwater sources prior to mixing with bofedal water was possible only at GW1 and GW3 (Figure 1b). GW1 represents a system of four springs discharging from the talus into the main SQC valley (site L1; Figure 1a). The talus is topographically disconnected from the glacier in the U1 subcatchment, appearing to be recharged by direct precipitation and run-off from the bedrock outcrop above (Figure S1c). The GW3 spring was identified and sampled in August 2022. GW3 originates from the south side of U1, approximately 50 m above the valley bottom on the south side of U1 and has no glacial sources above (Figure 1b).

Bofedal sampling was targeted to wetland pools in flatter, valley-bottom sites (sites L1, L2 and L3; Figure 1a) as well as in feeder tributary valleys with smaller bofedal areas and steeper slopes (sites U1, U2 and U3; Figure 1a). The quicker grab sampling of pools was preferred over subsurface sampling to maximize the sample size and to better represent the bofedal end-member thought to be more actively contributing to streamflow. Where possible, a systematic sampling approach was taken along cross-valley transects. The 89 'bofedal surface' (WS) grab samples were collected from the nearest bofedal pool to geolocated points. A second 'bofedal auger' (WA) sample was taken at 22 sites in August 2022 to investigate the similarity of the wetland pools to water in the nearby shallow subsurface. For these samples, a dry area of bofedal vegetation on a microtopographic high no more than 10 m from the WS sample was selected. A 50 cm soil plug was removed using a Russian peat corer and the hole allowed to refill for 2 min prior to sampling the water table.

Field measurements of SEC and temperature were made at the water source using a Mettler Toledo SevonGo SG7 conductivity metre, calibrated daily. Unfiltered samples were collected in HDPE bottles, stored out of direct sunlight and analysed within 6 months of collection. Analysis was carried out by isotope ratio (dual inlet) measurement on a Isoprime 100 mass spectrometer plus Aquaprep. Results obtained were expressed in permil (‰) with respect to VSMOW2 through repeated analyses of house standards (IAEA, 2017). Measurement errors for all samples were $\pm 0.05\%$ for $\delta^{18}\text{O}$ and $\pm 0.75\%$ for $\delta^2\text{H}$.

For all samples, the line-conditioned excess (Lc-excess) was calculated. Lc-excess defines the deviation of $\delta^{18}\text{O}$ and $\delta^2\text{H}$ with respect to the LMWL (Landwehr & Coplen, 2006) according to:

$$\text{Lcexcess} = \delta^2\text{H} - a\delta^{18}\text{O} - b$$

where a is the slope and b the intercept of the Pucarumi LMWL ($a = 7.98$; $b = 12.67$) defined by Guy et al. (2019). Where a LMWL is available for a given location, Lc-excess is a closer representation of post-depositional isotopic enrichment compared to d-excess (which defines the deviation of $\delta^{18}\text{O}$ and $\delta^2\text{H}$ only with respect to the

GMWL). The expectation is that water transiting bofedales will have a negative Lc-excess (due to the long transit times in the bofedales drainage network and opportunity for substantial evaporative enrichment at the near-surface) whilst dry season sources transiting to the river via other pathways will have an Lc-excess close to zero (indicating minimal evaporation).

3.5 | Identifying snowmelt and suitable periods for mixing analysis

Before quantification of the bofedal component of streamflow can be attempted using Lc-excess, the periods containing potential dynamic contributions from precipitation and snowmelt must first be excluded. On shorter timescales (e.g., days to months) incident precipitation shows significant deviation from the LMWL, therefore we restrict analysis to dry conditions where dynamic contributions from event-scale precipitation and snowmelt sources are negligible.

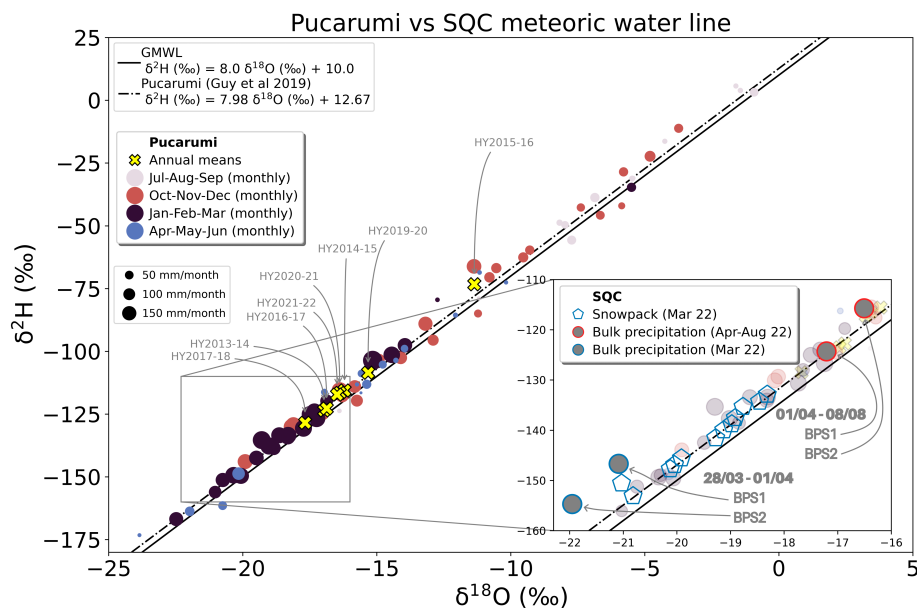
Rather than relying on lower elevation rain gauge data when on-glacier snow melt may not occur until sometime after the snowfall event, here we interrogate the characteristics of the diurnal AGS1 hydrograph to identify the influence of supraglacial snowmelt and define the transitions between different periods. The timing and form of the daily hydrograph melt peak can reveal important information about on-glacier processes over a melt season (Hannah et al., 2000; Irvine-Fynn et al., 2017). For example, a late peak may reflect the slow percolation of meltwater through a supraglacial snowpack covering the ablation zone. The paired principal component analysis (PCA) and hierarchical cluster analysis (HCA) approach of Hannah et al. (2000) was applied on the hourly water level measures on a 11 am–11 pm window at AGS1 from 2019 to 2022 (see SI S2 for further details). Lag times between air temperature at the AGS1 barometric sensor and water level in the pressure transducer were independently calculated to aid interpretation of hydrograph clusters, computed using a moving window cross correlation on the cleaned hourly dataset (Jobard & Dzikowski, 2006). Given the potential impact of englacial and proglacial as well as supraglacial processes on hydrograph form (Irvine-Fynn et al., 2017; Jobard & Dzikowski, 2006; Swift et al., 2005), all available meteorological, isotope and satellite data were synthesized together to aid interpretation of the periods and describe the catchment-scale water source dynamics.

3.6 | End-member mixing analysis

A downstream synoptic survey in the dry season from RL01 (>90% glacierized) to RL18/AGS2 (16% glacierized) showed the $\delta^{18}\text{O}$ - $\delta^2\text{H}$ signature was most similar to the glacial end-member along the whole river, though migrated appreciably toward the bofedal end-member with distance downstream.

For all identified periods where the RL18 isotopic signature was similar to the glacial end-member and event-scale rain and snowmelt contributions were not apparent, the fractional contribution of

FIGURE 2 Monthly mean and weighted annual mean $\delta^{18}\text{O}$ and $\delta^2\text{H}$ in precipitation at Pucarumi, 47 km NW of the SQC, for hydrological years (HY) 2013–21 (excl. HY 2018–19 for which data are not yet available) compared to SQC observations from March and August 2022. Size of Pucarumi monthly markers are proportional to rainfall amount.



bofedal runoff in streamflow at RL18 (F_{bofedal}) was quantified according to;

$$F_{\text{bofedal}} = (LC_{\text{RL18}} - LC_{\text{glacial}}) / (LC_{\text{bofedal}} - LC_{\text{glacial}})$$

where LC_{bofedal} is the lc-excess of a single sample selected from the normally distributed PDF of the bofedal end-member, LC_{glacial} is the lc-excess of a single sample randomly selected from the glacial end-member (the sample size was too small to estimate the parameters of the distribution), and LC_{RL18} the lc-excess of the selected RL18 sample corrected for evaporative enrichment. End-member sampling was only undertaken during the two intensive field sampling campaigns, rather than the interim period when the majority of the RL18 samples were collected, so time-varying end-member characterization was not possible. The evaporative correction was applied to estimate the lc-excess decrease caused by in-channel evaporation as water moves downstream in the main river stem (see SI S3 for further details). Monte Carlo sampling for each of the selected periods (iterations = 100 000) was used to investigate the impact of uncertainties in measurement, choice of LMWL (based on the coefficients published by Guy et al. (2019) for the 6 precipitation collection sites in the Vilcanota), end-member and in-channel evaporation assumptions.

4 | RESULTS

4.1 | Wet to dry season isotopic variability

4.1.1 | Precipitation

The stable isotope data show precipitation becomes increasingly depleted through the wet season, and more enriched in the dry

(Figure 2). The close proximity of the SQC snowpack and bulk sampler observations to the Pucarumi LMWL (Figure 2 inset) emphasizes the regionally-consistent precipitation dynamics and LMWLs (Guy et al., 2019). Evaporation from bulk samplers and sublimation of the late-March snowpack appears minimal.

The SQC samples closely match the short-term isotopic variability at Pucarumi (Figure 3a). SQC snowpack samples taken on 30th March have a mean $\delta^{18}\text{O}$ of $-18.86\text{‰} \pm 2.31^1$ (min = -21.03 , max = -11.40‰), and the SQC bulk samplers capture rainfall events the following week with more depleted $\delta^{18}\text{O}$ values of -21.95 and -21.09‰ . These samples correspond closely in trajectory and absolute value to the progressive $\delta^{18}\text{O}$ depletion at Pucarumi during March 2022. The SQC bulk precipitation samples (BPS) collected from April – August also closely match the daily Pucarumi observations aggregated over the same window. This agreement suggests that Pucarumi provides a good approximation of the isotopic variability on the weekly to seasonal scale within the catchment. The similarity (and slight enrichment) of the SQC BPS (4780–5112 m) compared to the Pucarumi (4150 m) observations is consistent with longer monitoring at the scale of the VUB which has not found evidence of an elevation effect (Guy et al., 2019).

The 2021–22 hydrological year was relatively wet compared to other years, with the highest annual precipitation (954 mm) at the shielded and heated Sabinacocha gauge since measurement began in 2017–18 (Table S1). Comparing the rain gauge records (Figure 3b), the seasonality is broadly comparable but differences in recorded precipitation amount could point either to local differences in rainfall or to monitoring biases (e.g., to systematic under-catch during hail events from the tipping bucket rain gauge in the SQC). For this reason, we considered other information sources (e.g., hydrograph analysis) when interpreting the influence of snowmelt/rainfall events rather than relying on SQC rain gauge data alone.

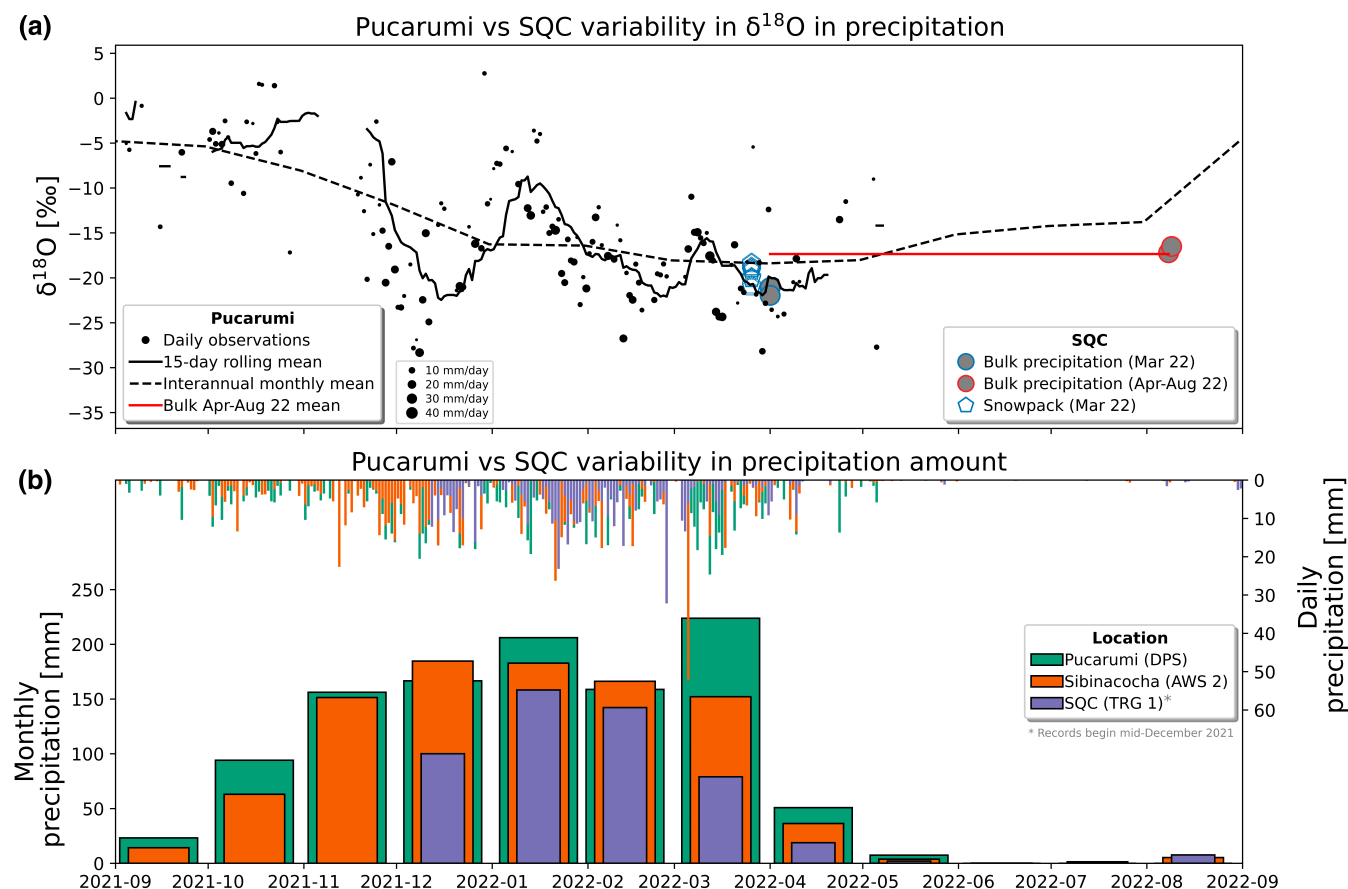


FIGURE 3 (a) Daily $\delta^{18}\text{O}$ precipitation observations at Pucarumi (black points, size indicates precipitation amount), 15-day rolling volume-weighted mean (black line) and monthly mean (black dashed line). (b) Cumulative monthly (left axis) and daily (right axis) precipitation comparison at Pucarumi, Sibinacocha and the SQC.

4.1.2 | Glacial melt

Glacial melt samples ($n = 7$) collected from proglacial melt streams and ice samples in March and August 2022 exhibit a $\delta^{18}\text{O}$ range of -17.33 to -15.70‰ (mean = $-16.54 \pm 0.67\text{‰}$), close to the weighted annual mean $\delta^{18}\text{O}$ of Pucarumi precipitation (mean = $-15.67 \pm 1.82\text{‰}$). All samples lie near the Pucarumi LMWL (Figure 4a) with a mean l_c -excess of 0.83 ± 0.45 (Table 1).

4.1.3 | Groundwater

Two perennial spring areas were sampled at source in the catchment at locations with no obvious mixing with other water sources (GW3 and GW1). GW1 springs, show a similar isotopic signature in both sampling seasons, with a mean $\delta^{18}\text{O}$ of -18.05‰ in March and -17.97‰ in August (Figure S12). The high l_c -excess of the springs (range -1.8 to 1.4 , mean = -0.4 ± 1.2) suggests minimal evaporation (Table 1).

4.1.4 | Bofedal and tributary samples

The WS (bofedal surface) samples show a consistent evaporative signal, with all samples falling to the right-hand side of the LMWL

(negative l_c -excess) in both sampling seasons (Figure 4a). The WS samples show the largest isotopic variability of all sample types with a $\delta^{18}\text{O}$ SD of 1.64‰ in March 2022 and 1.62‰ in August 2022 (Figure 4, Table S3). The WA (bofedal auger) samples are isotopically similar to the WS samples; however we find a statistically significant mean $\delta^{18}\text{O}$ enrichment of 0.67‰ (paired two-sample t -test, $p < 0.05$) of WS compared to WA (Table S5).

All WS in August from upper valley sites have a more positive l_c -excess than lower bofedal sites (mean L1 = -9.6 , L2 = -9.6 , L3 = -9.8 , U1 = -5.6 , U2 = -5.8). With the exception of site U3, the same pattern is observed in March (mean L1 = -9.0 , L3 = -13.5 , U2 = -2.0 , U3 = -10.9). Interestingly, in August the tributaries discharging from the upper into the lower valley sites (e.g., TR12-14, Figure 5a,b) have a negative l_c -excess similar to the bofedales in the upper valley. The tributaries further away from the glacial headwater (larger circles, Figure 4b,c), show an evaporative signature similar to the bofedal samples. Mean l_c -excess of the samples taken in the valley bottom bofedal sites (L1 and L3) are similar for the March and August sample campaigns, with an l_c -excess of -11.2 ± 5.7 in March and -9.7 ± 5.6 in August. A two-sample Kolmogorov-Smirnov test of the l_c -excess distributions over the two seasons showed that the null hypothesis that the L1 and L3 samples are drawn from the same underlying distribution could not be rejected ($p > 0.05$). Accordingly, the overall mean of the L1 and L3 samples in both seasons

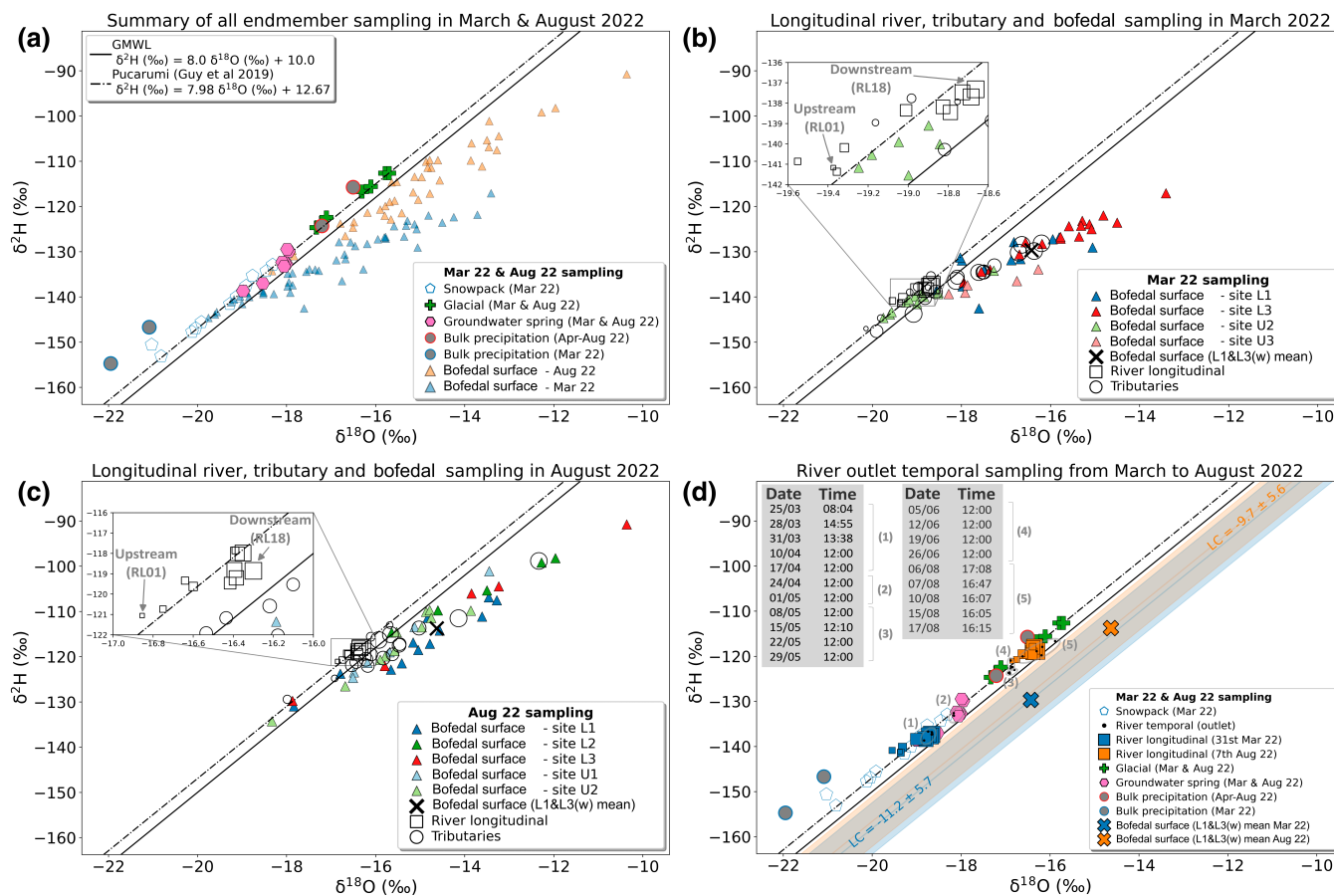


FIGURE 4 Stable isotope composition ($\delta^{18}\text{O}$ and $\delta^2\text{H}$) of waters sampled in March and August sampling campaigns (panels a–c) and temporal samples collected at RL18 during the interim period (panel d). For panels b–d ‘River longitudinal’ and ‘Tributary’ symbol size indicates distance along the main channel, with smallest sizes at Quisoquipina snout (RL01) and largest sizes closest to AGS2 (RL18). In panel d, the mean Lc-excess ± 1 SD of the bofedal end-member in March and August is also shown to demonstrate the similarity between the two sampling campaigns.

(-11.0 ± 5.5) was used as the representative end-member for bofedal water supplying the main river. The Lc-excess of tributaries TR12–14 discharging from the upper valley bofedal during August 2022 fall within or just outside the upper 1 SD limit of this distribution (min = -6.7 , max = -5.2). Compared to upper bofedal wetlands the lower bofedales were considered the more representative end-member for water entering the main river. This was due to their larger spatial extent, and because tributaries discharging the upper bofedales were often observed to supply the lower bofedales directly (e.g., TR13–14, Figure 1b), becoming indistinguishable from the distributed lower bofedal pond network on entering the main valley (Figure S1d).

4.1.5 | Longitudinal and temporal sampling of the main river

The isotopic composition of river samples shows a significant change between the March wet-season sampling ($\delta^{18}\text{O} = -19.00 \pm 0.28$, $\delta^2\text{H} = -138.8 \pm 1.4$, $n = 18$, Table S3) and August dry-season sampling ($\delta^{18}\text{O} = -16.41 \pm 0.23$, $\delta^2\text{H} = -119.1 \pm 1.2$, $n = 19$, Table S3) (two-sample t-test, $p < 0.05$). The longitudinal variability is smaller than the seasonal variability (Figure 4d), but a consistent enrichment

is observed with distance downstream in both March and August 2022, with an increase in $\delta^{18}\text{O}$ of 0.71‰ and 0.56‰ respectively. Lc-excess generally decreases with distance downstream in both sampling campaigns (Figure 5c). For 18 of the 20 RL18 samples Lc-excess is negative.

SEC increases downstream between Quisoquipina snout from 80 to $90 \mu\text{S}/\text{cm}$ to a peak of $\sim 220 \mu\text{S}/\text{cm}$ reached by points RL08 and RL13 in March and August respectively (Figure S13a,b). Sample RL08 is found at the end of the glacierized area, and an increase in SEC with distance downstream between RL01 and RL08 may be indicative of more intensive rock-water reactions occurring with the more recently exposed glacial sediments in the upper catchment, followed by a shift toward runoff inputs with less time in contact with bedrock and clastic material in the lower catchment.

4.2 | Spatio-temporal variability in streamflow source waters

Weekly isotope sampling at RL18, bracketed by the March and August 2022 end-member sampling campaigns, can elucidate the water source contributions during a particularly dynamic time of

TABLE 1 Lc-excess by sample type.

Type	Site	Mar-22						Aug-22						Mar and Aug 22					
		n	Mean	SD	Min	50%	Max	n	Mean	SD	Min	50%	Max	n	Mean	SD	Min	50%	Max
SN	All	17	0.9	1.5	-0.4	0.4	4.8	1	6.5		6.5	6.5	6.5	18	1.2	2.0	-0.4	0.4	6.5
PB	All							2	1.9	2.1	0.4	1.9	3.3	2	1.9	2.1	0.4	1.9	3.3
GL	All	1	1.0		1.0	1.0	1.0	6	0.8	0.5	0.0	0.8	1.4	7	0.8	0.5	0.0	0.9	1.4
GLi	All	1	1.0		1.0	1.0	1.0	2	0.3	0.5	0.0	0.3	0.7	3	0.6	0.5	0.0	0.7	1.0
GLs	All							4	1.1	0.3	0.8	1.0	1.4	4	1.1	0.3	0.8	1.0	1.4
GW	All	4	-1.3	0.6	-1.8	-1.4	-0.6	3	0.8	0.6	0.2	0.7	1.4	7	-0.4	1.2	-1.8	-0.6	1.4
RL	All	18	0.2	1.1	-1.3	0.1	2.6	19	-0.9	1.2	-3.2	-0.9	0.8	37	-0.4	1.3	-3.2	-0.1	2.6
TR	All	33	-3.9	3.7	-11.9	-3.9	1.5	25	-4.5	3.3	-13.1	-3.8	1.4	58	-4.1	3.5	-13.1	-3.9	1.5
WS	All	50	-9.5	6.9	-25.1	-8.9	0.4	39	-7.9	4.5	-20.7	-6.6	0.2	89	-8.8	6.0	-25.1	-8.1	0.4
WS	L1 and L3	29	-11.6	5.7	-22.7	-12.6	-0.1	17	-9.6	5.2	-20.7	-10.7	0.2	46	-10.9	5.6	-22.7	-11.2	0.2
WS	L1 and L3 (w)	29	-11.2	5.7	-22.7	-12.6	-0.1	17	-9.7	5.6	-20.7	-10.7	0.2	46	-11.0	5.5	-22.7	-10.6	0.2
WS	L1	12	-9.0	6.2	-21.6	-8.4	-0.1	12	-9.6	4.3	-15.2	-10.9	-1.3	24	-9.3	5.2	-21.6	-10.6	-0.1
WS	L2							5	-9.6	5.4	-15.4	-10.3	-2.5	5	-9.6	5.4	-15.4	-10.3	-2.5
WS	L3	17	-13.5	4.6	-22.7	-13.8	-6.2	5	-9.8	7.5	-20.7	-8.7	0.2	22	-12.7	5.4	-22.7	-13.1	0.2
WS	U1							6	-5.6	0.8	-6.5	-5.5	-4.6	6	-5.6	0.8	-6.5	-5.5	-4.6
WS	U2	12	-2.0	2.7	-9.0	-0.8	0.4	11	-5.8	2.8	-11.8	-6.4	-0.7	23	-3.8	3.3	-11.8	-3.9	0.4
WS	U3	5	-10.9	4.8	-16.7	-8.7	-6.1							5	-10.9	4.8	-16.7	-8.7	-6.1
WA	All							24	-7.3	3.8	-15.5	-6.9	-1.6	24	-7.3	3.8	-15.5	-6.9	-1.6
WA	L1 and L3							11	-10.0	3.5	-15.5	-9.3	-3.2	11	-10.0	3.5	-15.5	-9.3	-3.2
WA	L1 and L3 (w)							11	-9.6	2.9	-15.5	-9.9	-3.2	11	-9.6	2.9	-15.5	-9.9	-3.2
WA	L1							8	-10.5	4.1	-15.5	-9.9	-3.2	8	-10.5	4.1	-15.5	-9.9	-3.2
WA	L2							1	-9.2		-9.2	-9.2	-9.2	1	-9.2		-9.2	-9.2	-9.2
WA	L3							3	-8.7	0.7	-9.3	-8.8	-7.9	3	-8.7	0.7	-9.3	-8.8	-7.9
WA	U1							6	-4.1	2.5	-8.3	-4.2	-1.4	6	-4.1	2.5	-8.3	-4.2	-1.4
WA	U2							10	-4.9	1.2	-6.0	-5.5	-2.5	10	-4.9	1.2	-6.0	-5.5	-2.5

Note: Colour gradient extends from highest Lc-excess values in blue (LC = 6.5) to lowest in red (LC = -22.7).

Abbreviations: GL, glacial; GLi, glacier ice; GLs, glacier stream; GW, groundwater; PB, bulk precipitation; RL, main river; SN, snowpack; TR, tributary stream; WA, bofedal auger; WS, bofedal surface.

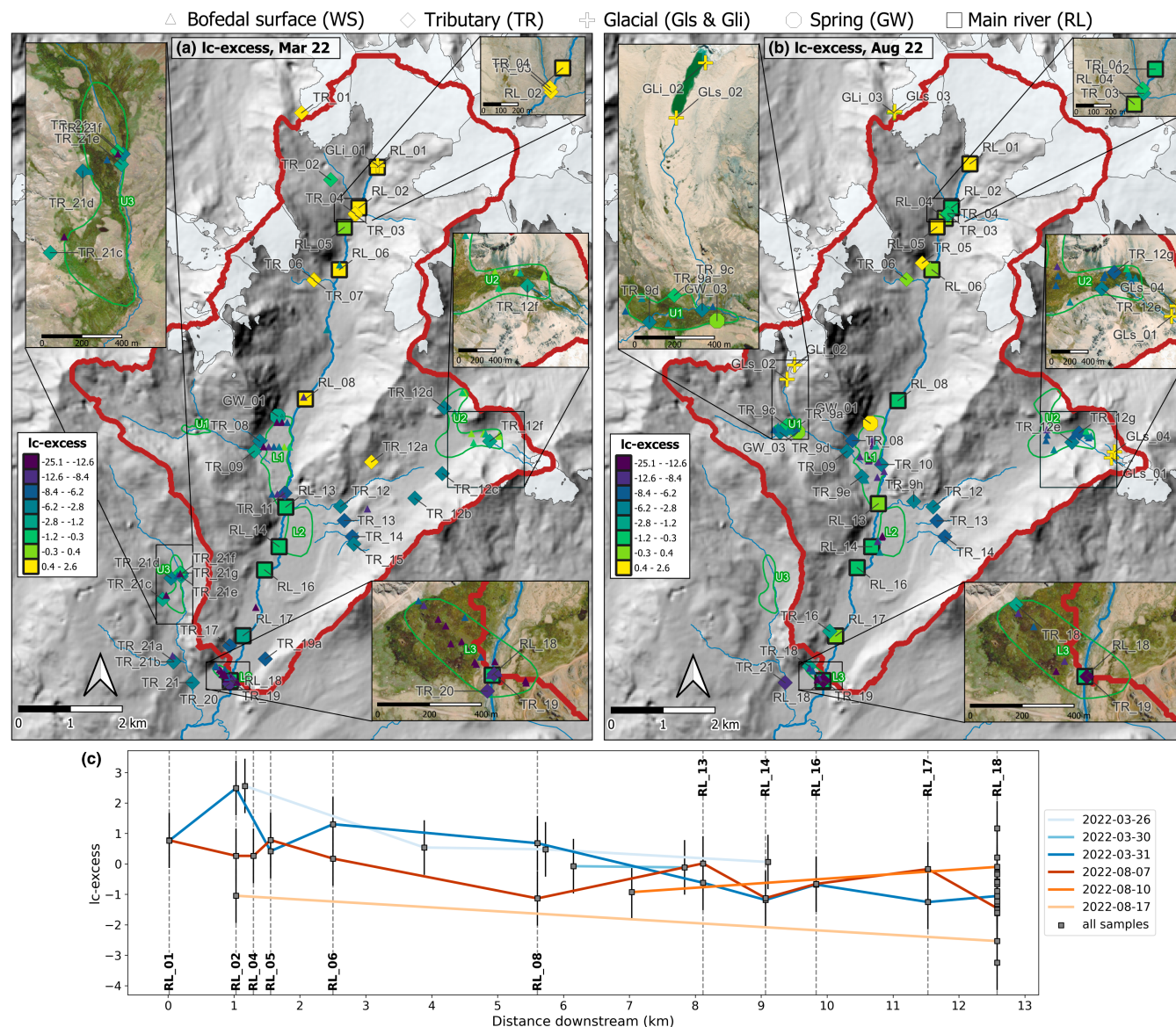


FIGURE 5 Spatial variability in Ic-excess for sampling campaigns in (a) March 2022 and (b) August 2022. For clarity only main channel samples from longitudinal sampling campaigns on the 31st March and 7th August are shown. Glacier and lake extent from 2020 inventory of (INAIGEM, 2023). Hillshade basemap generated from ALOS satellite (JAXA, 2021). (c) Trend in Ic-excess with distance downstream for all river samples ($n = 49$), colour coded where multiple samples were taken along the river on the same day. Main channel sampling locations are indicated for all samples taken on 31/03/2022 and 07/08/2022 (longitudinal sampling days).

the hydrological year. The RL18 range in $\delta^{18}\text{O}$ is -18.8 to -18.3% prior to 1st May and -16.9 to -15.9% thereafter (Table 1), indicating a shift in water sources during the transition from the wet to the dry season.

These changes are interpreted using Figure 6. Diurnal hydrograph classification of the 1071/1461 days with complete observations at AGS1 yielded three hydrograph groupings; ‘early’, ‘mid’ and ‘late’ daily peaks (SI S2.2). Four key periods are delineated based on the transitions between these clusters (Figure 6a) and are described below using evidence from: the daily lag between air temperature and discharge at AGS1 from the cross-correlation analysis (T-Q lag, Figure 6b), the glacial and non-glacial water level monitoring

(Figure 6c), the meteorological monitoring available at TRG1 and AWS1 (Figure 6d), the satellite-derived snow and ice cover fraction in the catchment (Figure 6e), and the isotopic changes at RL18 (Figure 6f.g).

4.2.1 | Period 1: ‘Frequent heavy precipitation’

The T-Q lag times and hydrograph clustering (Figure 6a,b) are characterized by inter-day switching between early and late peaked hydrographs over consecutive days. Daily precipitation totals are high with respect to other periods (Figure 6d). The hydrograph changes are

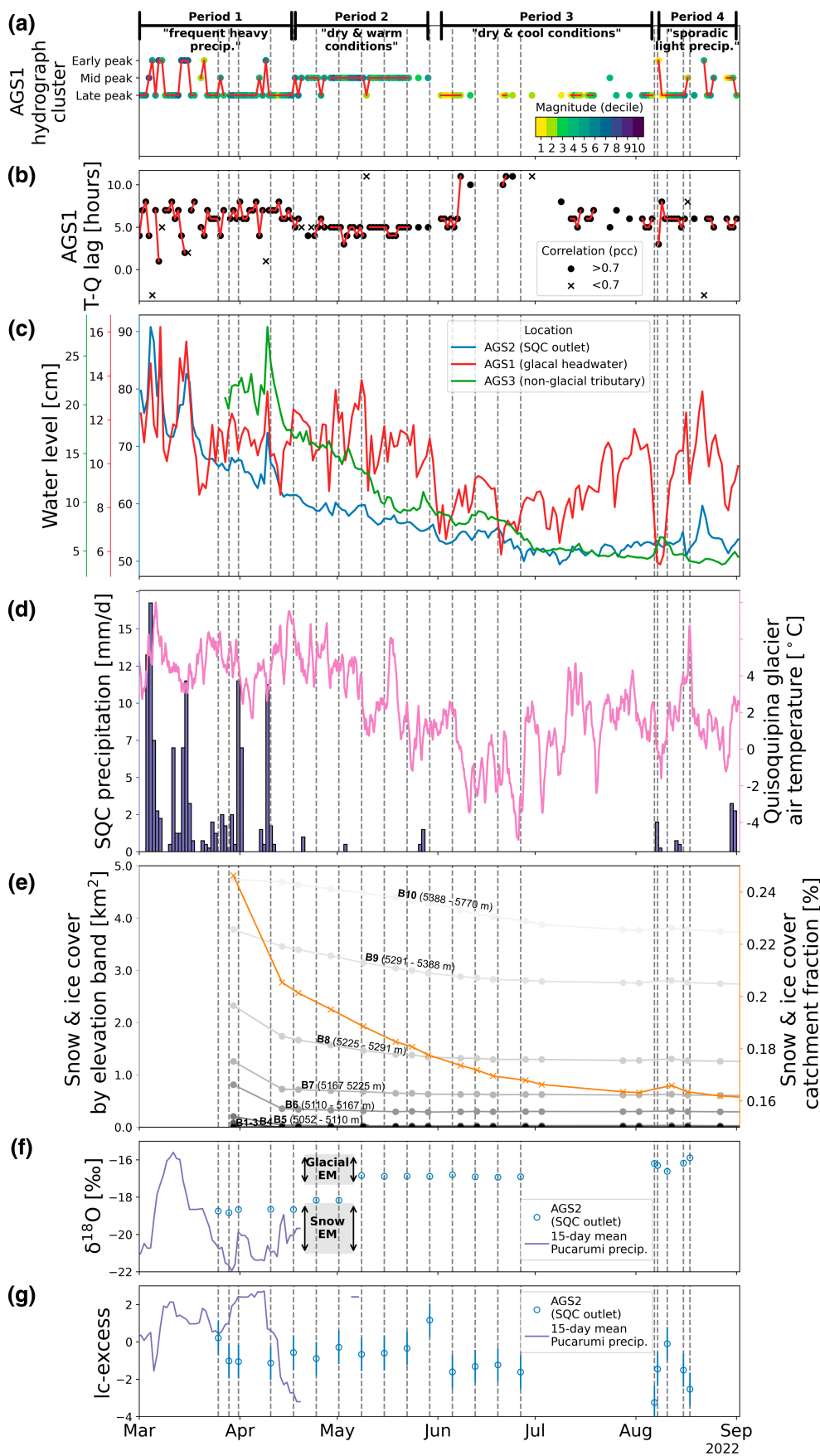


FIGURE 6 Wet to dry season temporal variability in; (a) hydrograph shape clusters; (b) diurnal hourly temperature – discharge lag at Quisoquipina glacier; (c) water level at AGS1, AGS2, and AGS3; (d) precipitation at SQC raingauge (RSG1) and temperature at Quisoquipina glacier (AWS1); (e) Snow and ice cover derived from SENTINEL2 satellite imagery in 10 equal area-weighted elevation bands. © European Space Agency – ESA; (f, g) δ¹⁸O and Ic-excess at RL18 (AGS2), with rolling-15 day precipitation mean and range of snow and glacial end-members shown for context.

frequent and rapid compared to the snow-ice transitions observed over longer time windows on alpine glaciers with seasonal snowpacks (Hannah et al., 1999), likely reflecting the transience of on-glacier snowcover and associated variability in albedo and ablation on different days and elevations on the glacier surface (Fyffe et al., 2021). The streamflow sample taken on 10/04 at RL18 captures the falling limb of the final storm event of the wet season in which a clear response in both glacial and non-glacial hydrographs is observed (Figure 6c). From 25/03 to 10/04 the isotopic signature at RL18 is similar to rainfall and snowpack samples at the end of the wet season (Figures 4d and 6f). The fractional area of snow and ice cover shows a large overall decrease during April (Figure 6e). Values are then static for the lowest 70% of elevations (4746–5225 m) for the remainder of the dry season, showing the rapid melt of off-glacier wet season snow cover at these elevations early in the dry season.

4.2.2 | Period 2: ‘Dry and warm conditions’

Period 2 is characterized by mid-peaked hydrographs with less frequent switching between clusters (Figure 6a). From 10/04 to 24/04, the T-Q lag time at AGS1 steadily transitions from 7 to 5 h (Figure 6b). From 17/04 to 08/05 the RL18 (AGS2) samples transition from an isotopic content similar to wet season precipitation to that of the ice melt end-member (Figure 6f). The increasing dominance of glacial sources during Period 2 is also indicated by the sustained high water level at AGS1 (glacial) even as AGS3 (non-glacial) continues a relatively steep recession (Figure 6c). Two isotope samples taken on 24/04 and 01/05 capture transitional points. This isotopic transition at AGS2 occurs 1–2 weeks after the T-Q lag time stabilizes at 5 h at AGS1 in the glacial headwaters (Figure 6b). RL18 samples collected on 08/05, 15/05 and 22/08 are isotopically similar to the glacial end-member, and represent a warm, dry period with no precipitation recorded at RSG1. Daily mean temperatures on the glacier between these dates vary from -1.6 to $+1.0^{\circ}\text{C}$ (mean = -0.7°C). A 1.6 mm precipitation event on 26–27/05 (Figure 6d, SI S5) is recorded at the end of Period 2 and the RL18 sample taken 2–3 days later on 29/05 showed an elevated Ic-excess compared to samples from drier dates (Figure 6g).

4.2.3 | Period 3: ‘Dry and cool conditions’

Late-peaked hydrographs characterize Period 3, and a water level reduction at AGS1 also coincides with the onset of the period (Figure 6a). During the dry season, at scales of greater than 1 week, water level at AGS1 appears to follow mean daily air temperature (Figure 6c,d). Daily mean temperatures are lower than in Period 2, and especially from 05/06 to 26/06 (mean = -2.6°C , range -4.4 to -0.9°C) when samples at RL18 were collected. Each sample taken at RL18 during Period 3 ($n = 4$) has a more negative Ic-excess than the samples from Period 2 ($n = 3$), with a mean difference of 0.9. Sampling on 06/08 marks the onset of a more dynamic period (Figure 6a, SI S5).

4.2.4 | Period 4: ‘Sporadic light precipitation’

Period 4 is marked by a similar switching between early, mid and late-peaked hydrographs as observed in Period 1 (Figure 6a). Sporadic precipitation events occur at the TRG1 gauge from 07/08 (Figure 6a,d). Although water level at AGS1 still appears to track air temperature changes, these precipitation events complicate interpretation of the more subtle changes in $\delta^{18}\text{O}$ - $\delta^2\text{H}$ at RL18, and the mixing of new snowmelt contributions with ice melt potentially drives some of the variability in Ic-excess (Figure 6g). However, AGS2 precipitation totals and water levels at AGS2 and AGS3 remain relatively low and generally characteristic of the dry season. RL18 $\delta^{18}\text{O}$ also remains similar to the glacial end-member (Figures 4d and 6f).

4.3 | Bofedal contributions to streamflow

To take a conservative approach to identifying bofedal contributions to streamflow, we removed samples where event-scale rain/snowmelt contributions were potentially driving isotopic variability at RL18. We excluded samples from; periods characterized by precipitation events (Periods 1 and Period 4); less than two-days after a recorded rain event (29/05/2022 sample); during the wet-dry season freshet identified by changing diurnal lag time at the glacier snout and $\delta^{18}\text{O}$ - $\delta^2\text{H}$ similarity at RL18 to late wet season snow (24/04/2022 and 01/05/2022 samples). This yielded 7 out of 20 RL18 samples for subsequent analysis (08/05, 15/05, 22/05, 05/06, 12/06, 19/06, and 26/06/2022).

The $\delta^{18}\text{O}$ - $\delta^2\text{H}$ of the RL18 samples for these dates indicate that glacial melt is the dominant water source to the river (Figures 4d and 6f). End-member sampling shows an $\delta^{18}\text{O}$ - $\delta^2\text{H}$ enrichment (Ic-excess decrease) with distance downstream and a migration toward bofedales and bofedal-fed tributaries which cannot be explained by any other end-members sampled in March or August 2022 (Figure 4). Campaign sampling of glacial and bofedal sources was not undertaken when any of the 7 samples were collected in May–June 2022, however the consistency of Ic-excess of glacial and bofedal end-members in both March and August 2022 (overlapping shaded bands in Figure 4d) suggests the intermediate period is adequately characterized by the bracketing sample campaigns. The bofedal end-member was characterized using samples collected in August 2022 at lower valley sites L1 and L3, and the glacial using all available glacial samples (Table 1).

Across all samples, the median fractional bofedal contribution is 0.09–0.20 (± 0.09 –0.10) (Figure 7a). Bofedal outflow is stable, and the fractional increase in bofedal supply between Period 2 and Period 3 is driven mainly by the reduction in overall discharge caused by lower supply from glacial sources (Figure 7b).

5 | DISCUSSION

In wet and dry seasons, we found an increasing enrichment of $\delta^{18}\text{O}$ and $\delta^2\text{H}$ (increasing Ic-excess) with distance downriver in the SQC (Figures 4d

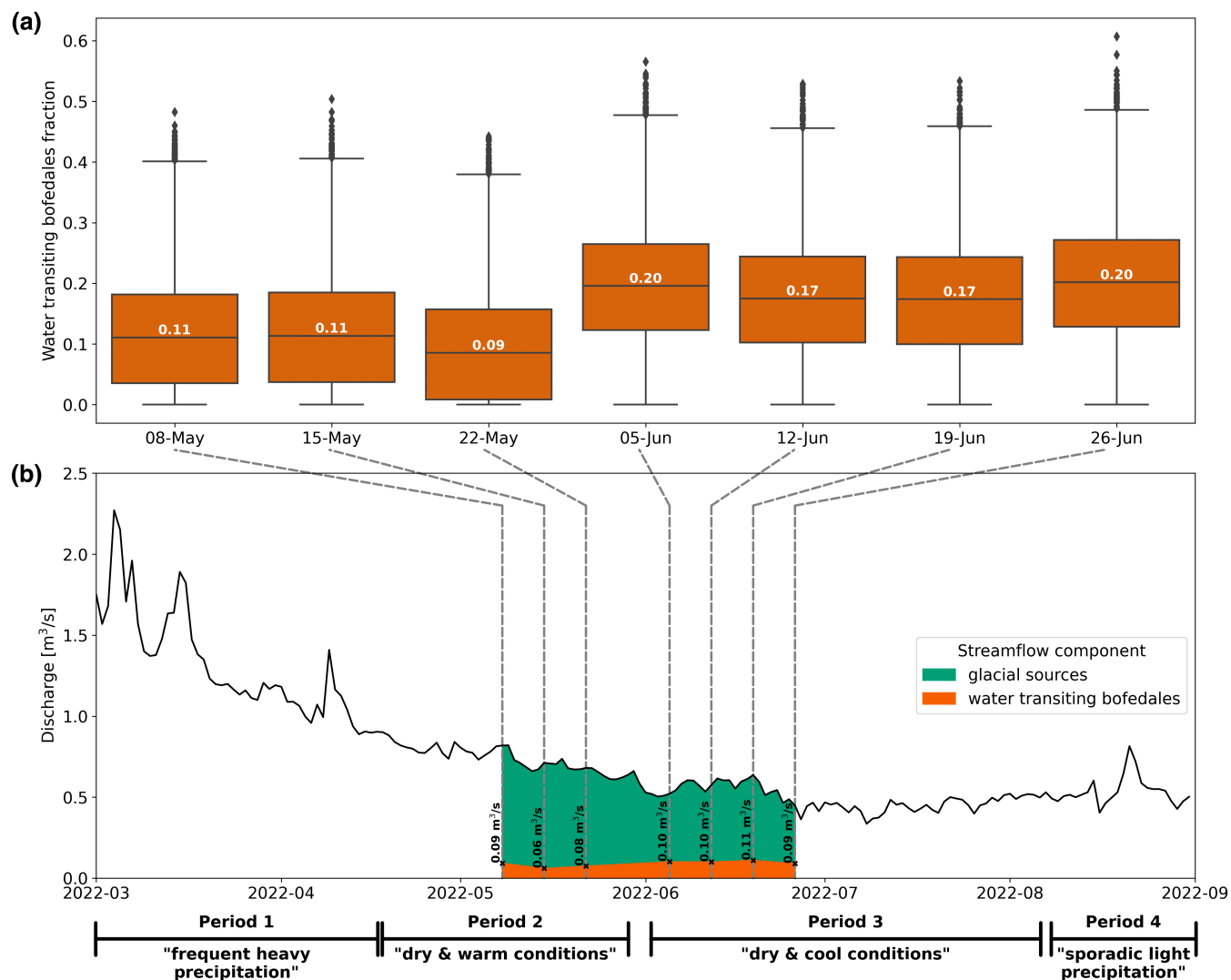


FIGURE 7 (a) relative contributions of water transiting bofedales and glacial sources at AGS2 based on two-component mixing model and Monte Carlo uncertainty analysis. Boxplot represents 25th – 75th percentiles (white text indicates median value) and whiskers extend to $1.5 \times$ interquartile range. (b) Absolute contributions of water transiting bofedales and glacial sources calculated by applying median fractional contributions to AGS2 discharge.

and 5c). We suggest that during certain dry periods, Ic-excess can be used to separate the streamflow contributions of glacial and bofedal water source dynamics, before introducing a conceptual model that includes the broader groundwater system to aid discussion of the implications (and limitations) of our findings in this rapidly deglaciating landscape.

5.1 | Dry season glacial melt dynamics

The seasonal evolution of stable isotopes at RL18 (AGS2 gauge) between March and August 2022 largely reflects the transition from wet season rain/snow to ice melt sources (Figures 4d and 6f). The steady $\delta^{18}\text{O}$ values at RL18 in Period 2 and 3 suggests a well-mixed glacial signal is reached after a 3 week period of transition following the last significant precipitation. Off-glacier snow cover in the SQC

does not persist for more than a few days after the end of the wet season except at the highest elevations. The T-Q lag of the AGS1 hydrograph in the highly glacierized upper part of the catchment supports our interpretation of a rapid transition from the longer flow-paths associated with meltwater percolating through the supraglacial snowpack to the shorter lag times of a more snow-free glacier surface. This transition is rapid compared to other studies worldwide (Aizen et al., 1996; Ohlanders et al., 2013; Penna et al., 2017), but concurs with the point-scale energy balance modelling in our catchment by Fyffe et al., 2021. The authors found an extremely thin maximum mean monthly snow depth of just 2 cm at AWS1, and that May–October contributions to total ablation were dominated by ice melt (76%), with snow melt (17%) and sublimation (7%) only minor contributors over the period. The 1–2 week difference between the stabilization of the T-Q lag time at AGS1 and the isotopic transition at AGS2 to that of an ice end-member could indicate catchment scaling effects

and/or the more delayed drainage of wet season precipitation from non-glacial stores downstream in the catchment.

Particular attention should be given to the melt contribution of the seasonal glacial snowpack because of the potentially high isotopic variability and associated uncertainty (Dar et al., 2024; Haiyan et al., 2018). During snowmelt, lighter isotopes are initially preferentially flushed and meltwater typically becomes progressively enriched over the snowmelt period (Beria et al., 2018; Lee et al., 2010; Noor et al., 2023; Stichler et al., 2001; Taylor et al., 2001). This is often due to the occurrence of liquid-ice fractionation, but further enrichment can occur due to isotopic fractionation by evaporation/sublimation (Lee et al., 2010; Noor et al., 2023; Taylor et al., 2001). On other glaciers with thin, transient snowpacks, the extent of isotopic fractionation in meltwaters is minimal, due to the large contributions from bare surface ice which do not introduce isotopic fractionation (Zhou et al., 2014). Liquid-ice fractionation is also thought to be lower under conditions of high melt rate (Noor et al., 2023). The seasonally consistent downriver enrichment (Figure 6) indicates that an off-glacier progressive enrichment is the likely driver in the SQC, however without samples from the glacier snout between Period 2 and Period 3 it is difficult to definitively exclude on-glacier fractionation processes during this period, despite the daily evaporation estimates remaining similar over this transition (Figure S11). For example, it is possible that the subtle enrichment in $\delta^{18}\text{O}$ - $\delta^2\text{H}$ (lc-excess decrease) at RL18 in Period 3 relate to the increased proportion of enriched snowmelt following a snow event on glacier at the end of Period 2. Penn et al. (2023) hypothesise that longer meltwater transit time during periods of snow cover may lead to enhanced evaporative fractionation compared to periods with more exposed surface ice when supraglacial drainage is more efficient. Whilst the lower water levels at AGS1 in Period 3 may reflect the persistently high albedo conditions following such a snowfall event, it may be that the ongoing seasonal decline in air temperature has reduced the absolute glacial contributions at AGS1 and therefore the relative contributions of non-glacial evaporative sources at AGS2 have increased. Improved understanding of glacier surface energy balance dynamics is required to predict how climate induced changes to precipitation amount, phase and timing will impact streamflow variability in glacierized Andean catchments. Future glacier modelling work will attempt to distinguish between snow and ice melt components to explore the significance of such dry season snow events.

5.2 | Bofedal and tributary stream fractionation signal

Wetlands often show extremely variable isotopic composition even within the same catchment (e.g., Cooper et al., 2019; Lahuatte et al., 2022; Sprenger et al., 2017), and in particular enrichment where the water table is closer to the surface and more exposed to radiation (Isokangas et al., 2017; Mayernik et al., 2024; Vyse et al., 2020). In the SQC, sampling was targeted in upper (U1, U2 and U3) and lower (L1, L2 and L3) valley bottom sites where bofedal wetland pools are

widespread even during the dry season (Figure S1d). A clear evaporative signal was observed in wet and dry seasons (Figure 4). The paired auger samples nearby to bofedal pools have slightly lower $\delta^{18}\text{O}$ than the pools themselves (Table S5), likely indicating that the pools are driving the evaporative fractionation and that subsequent mixing is occurring in the shallow groundwater (Vyse et al., 2020).

An evaporative signal is not always observed in tropical wetlands (e.g., Mosquera et al., 2016; Valois et al., 2021). Extensive monitoring at the Zhucaray experimental catchment in Ecuador has shown that wetland and streamwaters undergo only minimal fractionation, despite the majority of water draining through wetlands in both high and low flow conditions, probably due to high humidity (>90%) suppressing evaporation (Mosquera et al., 2016; Pesántez et al., 2023). In higher latitudes, temporal switching from high to low lc-excess in wetlands has been explained by changes between 'rainfall driven' and 'radiation driven' conditions (Sprenger et al., 2017). In the SQC, it is interesting that wetlands remain evaporatively enriched even during the wet antecedent conditions of March 2022 when larger contributions from more recent high lc-excess precipitation might be expected (Figure 4). The consistent evaporative enrichment may highlight the high year-round radiative forcing at our high-elevation tropical site. Alternatively, the shorter transit times in wet antecedent conditions may allow less time for evaporation, counterbalancing the increased exposure to evaporation from higher water tables and greater wetland contributing area.

The dominant water source supplying the sampled bofedales can be approximated assuming that the general bofedal $\delta^{18}\text{O}$ - $\delta^2\text{H}$ relationship reflects the local evaporation line along which the water has evolved (SI S6). At all sites, wet season bofedal water is similar to the late wet season precipitation end-member, and dry season wetland water similar to the groundwater springs discharging along the valley sides (Figure S17). This indicates ongoing groundwater supply to the bofedales during the dry season rather than simply a filling up of bofedales in the wet season followed by discharge in the dry. Similar to Cooper et al. (2019), our results highlight the general importance of groundwater supply even in glacierized headwaters, although the observed channel diversions from the main river (e.g., Figure S1b) may also provide an important supply in localized areas.

The evaporative signature of tributary streams TR12-TR14 suggests ongoing supply from upper valley bofedal sources well into the dry season (Figure 4). Even in catchments where strong evaporative enrichment of unsaturated soils occurs, streamwater and groundwater do not usually show signs of significant fractionation (Brooks, 2015; Evaristo et al., 2015; Sprenger et al., 2016), and fractionation of downstream waters is typically caused by evaporation of hydrologically connected surface water and saturated soils (Brooks et al., 2018). Calculated absolute bofedal contributions remain remarkably similar despite the large discharge decrease between Period 2 and 3 (Figure 7). This implies that a dynamic equilibrium has been reached between bofedal inflow and outflow during this window in the dry season. Other studies across different post-glacial landscapes have also shown continuing wetland connectivity to the downstream network during dry conditions. Brooks et al. (2018) examined

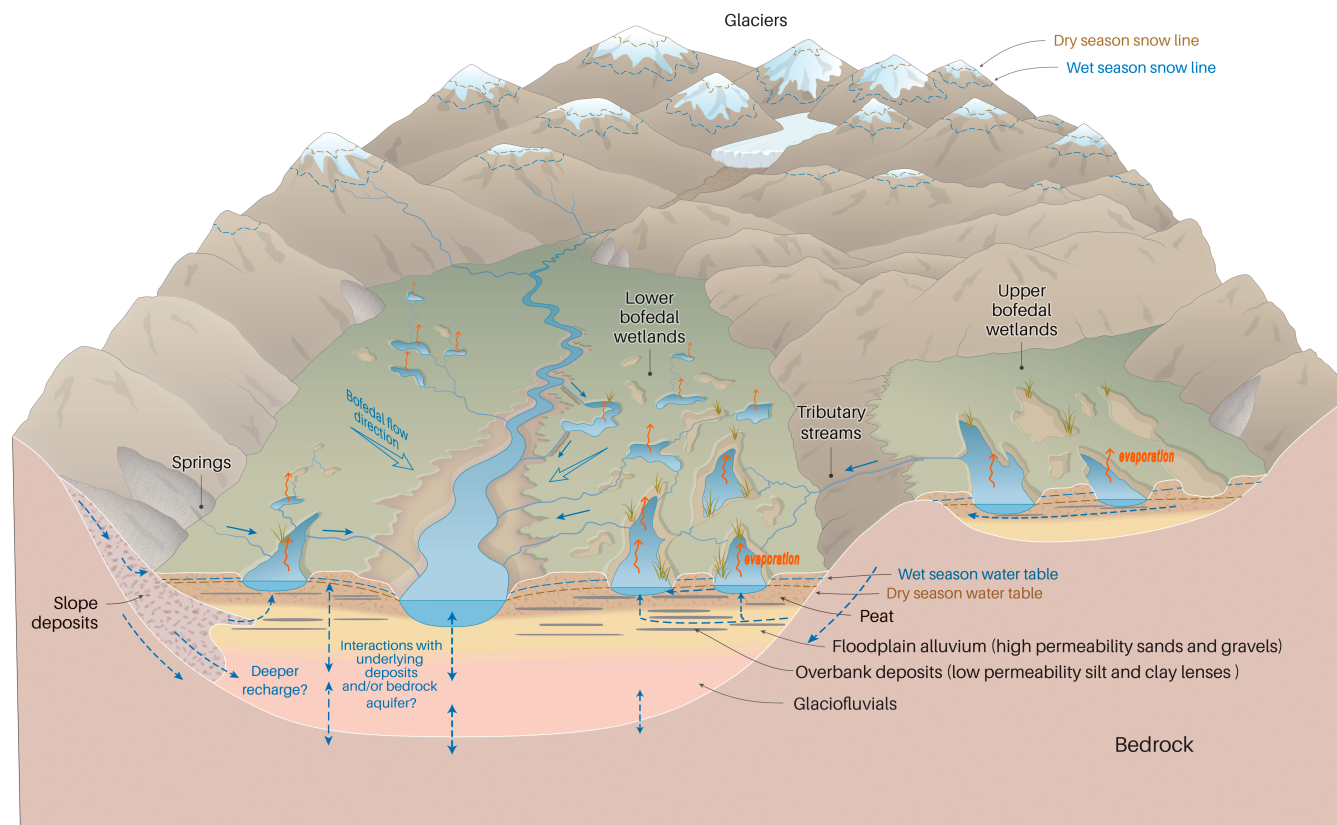


FIGURE 8 Conceptual model of the SQC showing ongoing bofedal wetland connectivity to the main river during the dry season drawing on other conceptual models from other analogue settings (Baraer et al., 2015; Ó Dochartaigh, Archer et al., 2019; Vyse et al., 2020; Wunderlich et al., 2023). Bofedales are supplied predominantly by groundwater. Springs emanating from hillslopes and slope deposits provide supply at the valley sides. Deeper groundwater exchanges are also possible between the peat and the underlying aquifers. Bofedal flow describes surface flow in the interconnected pond network as well as flow through the peat in the shallow subsurface.

wetland-stream connectivity in a watershed dominated by prairie-pothole wetlands and found ongoing contributions during baseflow conditions that cannot be explained by fill-and-spill processes activated during precipitation events. In the Scottish Bruntland Burn catchment, Sprenger et al. (2017) also demonstrated a passing on of the wetland signal to tributary streams during dry summer conditions, although Soulsby et al. (2021) showed that during an extended drought wetland contributions eventually ceased and downstream changes instead tended toward unevaporated groundwater contributions.

5.3 | Conceptual understanding of bofedal streamflow contributions

In Figure 8 we present our conceptual model describing the ongoing bofedal wetland contributions to streamflow in the SQC. The bofedal water table falls following the wet season, but remains sufficiently high to sustain saturated conditions for the duration of the dry season in some bofedal pools. This ensures that high evaporative fluxes and connectivity to the stream network is maintained year-round. We suggest supply to bofedales is maintained by groundwater discharging

from hillslope springs and slope deposits at the valley edges, and also potentially at larger distances from the hillslopes where localized upward head gradients occur allowing groundwater discharge from the underlying gravels through discontinuous clay lenses (e.g., Baraer et al., 2015; Ó Dochartaigh, Archer et al., 2019). The gently sloping topographic gradient, which is down-valley and toward the main river in the lower bofedales, connects bofedal pools in series as an expansive network of ‘flow-through’ wetlands (Leibowitz et al., 2016; Van Der Kamp & Hayashi, 2009). Pools are connected by peat flow in the shallow subsurface and through small channels between the pools where the water table is sufficiently high. The lower elevation sites L1, L2 and L3 have a lower I_c -excess compared to sites U1, U2 and U3, potentially suggesting further water cycling at larger scales as wetlands at higher elevation supply downstream wetlands in the main valley (Vyse et al., 2020). The lower SEC of samples at site U2 in March and August 2022 compared to L1 and L3 is also consistent with increased shallow groundwater entrainment of solutes from weathered material on these longer flow paths (Figure S13a,b).

The implicit assumption of our I_c -excess mixing approach is that all non-glacial groundwater contributing to streamflow transits through bofedales on route to the river. The similar I_c -excess of upper bofedales and streams discharging the tributary valleys suggest this is

a reasonable assumption in the upper valleys (Figure 5b). The available groundwater spring samples, though extremely limited in number, also support this assumption. The $\delta^{18}\text{O}$ - $\delta^2\text{H}$ position of the sampled talus and hillslope springs suggest that water is not contributing directly from these stores without first transiting through wetlands (Figure 4d). Studies in the CB have emphasized the importance of valley side deposits in sustaining groundwater springs in the dry season (Baraer et al., 2015), and as key zones of recharge for the underlying aquifer (Glas et al., 2019). We suggest a similar role for slope deposits in the SQC (Figure 8), though they are not as ubiquitous as the CB which may also explain the difficulty we had in locating spring sources. Lateral talus slopes supplied 9/11 of the springs sampled by Baraer et al. (2015) along the steep CB valley of Quilcayhuanca. If deeper groundwater stores in the SQC are isotopically similar to the few talus springs we sampled, direct contributions from deeper stores would be similarly unable to explain the downstream $\delta^{18}\text{O}$ - $\delta^2\text{H}$ river signal in the dry season (Figure 4d). Similar to other mountainous headwaters, deeper groundwater may be bypassing higher-order streams and supplying rivers only at a larger scale downstream (Frisbee et al., 2011; Gleeson & Manning, 2008; Hayashi, 2020), with flow primarily parallel to the SQC valley.

However, the isotopic content and connection between channel, floodplain, and the underlying glaciofluvial aquifer remains undetermined in the SQC, and substantial exchanges may occur at the interfaces (MacDonald et al., 2016; Mackay et al., 2020; Ó Dochartaigh, Archer et al., 2019). Indeed, some of the annual volume-weighted rainfall $\delta^{18}\text{O}$ - $\delta^2\text{H}$ values (Figure 2) overlap with the glacial samples (Figure 4d), which could indicate that deeper groundwater stores are isotopically indistinguishable from the glacial end-member (assuming that the groundwater signature reflects the volume-weighted precipitation over longer time periods). In such an instance, the 'glacial sources' component of Figure 7 would also represent an unknown contribution of non-glacial groundwater. Whilst this would mean our study overestimates the true glacial melt component, in the study of Baraer et al. (2015) the opposite is more likely because the authors do not distinguish between glacially and non-glacially derived groundwater sources in their two-component mixing analysis of melt and groundwater contributions using non-conservative tracers. The differences in end-member conceptualisation may explain why the melt component is only 49–62% of streamflow in the similarly glacierized (17%) and sized (71.5 km²) Quilcayhuanca valley compared to our assessment of 80%–91% in the SQC.

Our results differ to a greater extent to those of Ross et al. (2023) in the SQC, who suggest that glacial melt contributions are as low as 12% of streamflow during the 2020 dry season at AGS2. Our approach was generally to circumvent some of the uncertainties of the hydrometric methods employed in that study, although our finding that dry season flows are greatly augmented by the presence of glaciers is tentatively supported by spot gauging measurements. Salt dilution discharge measurements were made at AGS1 and AGS2 for two dry season dates in 2022. The discharge measurements show that AGS1 represents 37% (07/08/2022: AGS1 = 135 L/s, AGS2 = 366 L/s) and 40% (27/08/2022: AGS1 = 155 L/s,

AGS2 = 389 L/s) of the flow at AGS2, with 76% of the AGS2 glacial area remaining downstream of AGS1. Further work in the SQC will use tracer-aided glacio-hydrological modelling to better constrain the variability of stable isotopes and water fluxes in the different stores across multiple years, and will consider the role of surface water – groundwater exchanges which can be significant in these settings (Gordon et al., 2015; Somers et al., 2016).

6 | CONCLUSION

Isotope sampling revealed a rapid transition in the SQC over a period of 3 weeks from a flow regime dominated by recent rainfall and snow-melt to an ice-melt dominated system. We link the consistent downstream fractionation in surface water in the proglacial area to the contributions of bofedal wetlands. Similar to other conceptual models in the tropics (Mosquera et al., 2016; Wunderlich et al., 2023), we suggest that groundwater contributions at the scale of the SQC transit through a bofedal store before supplying the main channel. A simple two-component mixing model using Ic-excess to separate glacial and wetland components suggests dry season wetland contributions of between 9% and 20% ($\pm 9\%$ –10%) of total streamflow. Though the water resource impacts of adaptation strategies involving bofedales (e.g., FAO, 2022a; FAO, 2022b) remain poorly understood (Drenkhan et al., 2023), the high proportion of glacial melt that we find in this study suggests it will be challenging for any intervention to fully buffer the magnitude of the glacial melt reductions expected in the coming decades in the headwaters of the VUB (e.g., Mackay et al., 2024). On the other hand, the ongoing supply from bofedales long into the dry season suggests that adaptation measures that modify bofedal hydrology beyond the headwaters could have important impacts on water resources regionally and should be further explored.

ACKNOWLEDGEMENTS

Tom Gribbin was supported by the CENTA doctoral training programme (NERC grant no. NE/S007350/1) and CONDESAN. Fieldwork was also enabled by the RAHU project (NERC grant no. NE/S013210/1). J Mackay and A MacDonald contributed via the BGS International NC programme 'Geoscience to tackle Global Environmental Challenges' (NERC reference NE/X006255/1). The authors thank Adrian Ccahuana Condori, Alfredo Ccahuana and Anselmo Condori Alanocca, David Mendoza and the Phinaya community for their invaluable support of fieldwork, and citizen scientists Nelson Lozano and Felipe Crispin for their sampling efforts. Fabian Drenkhan of PUCP is thanked for their practical support and insights into tropical glacial hydrology. Josh West and Shreya Ramesh (University of Southern California) and Carol Arrowsmith (BGS, NEIF grant no. 2573) helped with stable isotope analysis. We are grateful to use meteorological data provided by SENAMHI. We also thank Bethan Davies for useful comments on an earlier manuscript version, and for the anonymous reviewers whose comments greatly improved the final manuscript. This paper is published with the permission of the Director, British Geological Survey (UKRI).

DATA AVAILABILITY STATEMENT

The data that support the findings of this study are available from the corresponding author upon reasonable request.

ORCID

Tom Gribbin  <https://orcid.org/0009-0001-6905-5822>

Jonathan D. Mackay  <https://orcid.org/0000-0003-4373-5747>

Alan MacDonald  <https://orcid.org/0000-0001-6636-1499>

David M. Hannah  <https://orcid.org/0000-0003-1714-1240>

Wouter Buytaert  <https://orcid.org/0000-0001-6994-4454>

Jan R. Baiker  <https://orcid.org/0000-0002-2634-0690>

Nilton Montoya  <https://orcid.org/0000-0002-4147-2579>

L. Baker Perry  <https://orcid.org/0000-0003-0598-6393>

Anton Seimon  <https://orcid.org/0000-0001-7326-0442>

Maxwell Rado  <https://orcid.org/0000-0002-7848-7926>

Sandro Arias  <https://orcid.org/0000-0002-8747-4895>

ENDNOTE

¹ In this paper ± indicates the standard deviation.

REFERENCES

- Aizen, V. B., Aizen, E. M., & Melack, J. M. (1996). Precipitation, melt and runoff in the northern Tien Shan. *Journal of Hydrology*, 186, 229–251.
- Amatulli, G., García Marquez, J., Sethi, T., Kiesel, J., Grigoropoulou, A., Üblacker, M. M., Shen, L. Q., & Domisch, S. (2022). Hydrography90m: A new high-resolution global hydrographic dataset. *Earth System Science Data*, 14, 4525–4550.
- Baraer, M., Mckenzie, J., Mark, B. G., Gordon, R., Bury, J., Condom, T., Gomez, J., Knox, S., & Fortner, S. K. (2015). Contribution of groundwater to the outflow from ungauged glacierized catchments: A multi-site study in the tropical Cordillera Blanca, Peru. *Hydrological Processes*, 29, 2561–2581.
- Beria, H., Larsen, J. R., Ceperley, N. C., Michelon, A., Vennemann, T., & Schaeffli, B. (2018). Understanding snow hydrological processes through the lens of stable water isotopes. *WIREs Water*, 5, e1311.
- Bertassello, L. E., Rao, P. S. C., Jawitz, J. W., Aubeneau, A. F., & Botter, G. (2020). Wetlandscape hydrologic dynamics driven by shallow groundwater and landscape topography. *Hydrological Processes*, 34, 1460–1474.
- Brooks, J., Mushet, D., Vanderhoof, M., Leibowitz, S., Christensen, J., Neff, B., Rosenberry, D., Rugh, W., & Alexander, L. (2018). Estimating wetland connectivity to streams in the Prairie Pothole Region: An isotopic and remote sensing approach. *Water Resources Research*, 54, 955–977.
- Brooks, J. R. (2015). Water, bound and mobile. *Science*, 349, 138–139.
- Burns, D. A., & McDonnell, J. J. (1998). Effects of a beaver pond on runoff processes: Comparison of two headwater catchments. *Journal of Hydrology*, 205, 248–264.
- Buytaert, W., & Beven, K. (2011). Models as multiple working hypotheses: Hydrological simulation of tropical alpine wetlands. *Hydrological Processes*, 25, 1784–1799.
- Buytaert, W., Cuesta-Camacho, F., & Tobón, C. (2011). Potential impacts of climate change on the environmental services of humid tropical alpine regions. *Global Ecology and Biogeography*, 20, 19–33.
- Buytaert, W., Moulds, S., Acosta, L., De Bievre, B., Olmos, C., Villacis, M., Tovar, C., & Verbist, K. M. (2017). Glacial melt content of water use in the tropical Andes. *Environmental Research Letters*, 12, 114014.
- Caballero, Y., Jomelli, V., Chevallier, P., & Ribstein, P. (2002). Hydrological characteristics of slope deposits in high tropical mountains (Cordillera Real, Bolivia). *Catena*, 47, 101–116.
- Chesnokova, A., Baraer, M., Laperrière-Robillard, T., & Huh, K. (2020). Linking mountain glacier retreat and hydrological changes in south-western Yukon. *Water Resources Research*, 56, e2019WR025706.
- Cooper, D. J., Sueltenfuss, J., Oyague, E., Yager, K., Slayback, D., Caballero, E. M. C., Argollo, J., & Mark, B. G. (2019). Drivers of peatland water table dynamics in the central Andes, Bolivia and Peru. *Hydrological Processes*, 33, 1913–1925.
- Cooper, D. J., Wolf, E. C., Colson, C., Vering, W., Granda, A., & Meyer, M. (2010). Alpine peatlands of the Andes, Cajamarca, Peru. *Arctic, Antarctic, and Alpine Research*, 42, 19–33.
- Dangles, O., Rabatel, A., Kraemer, M., Zeballos, G., Soruco, A., Jacobsen, D., & Anhelme, F. (2017). Ecosystem sentinels for climate change? Evidence of wetland cover changes over the last 30 years in the tropical Andes. *PLoS One*, 12, e0175814.
- Dar, T., Rai, N., Kumar, S., & Bhat, M. A. (2024). Understanding hydrological processes of glacierized catchments in the western Himalayas by a multi-year tracer-based hydrograph separation analysis. *Hydrological Processes*, 38, e15083.
- Drenkhan, F., Buytaert, W., Mackay, J. D., Barrand, N. E., Hannah, D. M., & Huggel, C. (2023). Looking beyond glaciers to understand mountain water security. *Nature Sustainability*, 6, 130–138.
- Drenkhan, F., Huggel, C., Guardamino, L., & Haerberli, W. (2019). Managing risks and future options from new lakes in the deglaciating Andes of Peru: The example of the Vilcanota-Urubamba basin. *Science of the Total Environment*, 665, 465–483.
- Dussailant, I., Berthier, E., Brun, F., Masiokas, M., Hugonnet, R., Favier, V., Rabatel, A., Pitte, P., & Ruiz, L. (2019). Two decades of glacier mass loss along the Andes. *Nature Geoscience*, 12, 802–808.
- Emmer, A. (2024). Infilled lakes (Pampas) of the cordillera Blanca, Peru: Inventory, sediment storage, and paleo outbursts. *Progress in Physical Geography: Earth and Environment*, 48(2), 208–230.
- Endries, J. L., Perry, L. B., Yuter, S. E., Seimon, A., Andrade-Flores, M., Winkelmann, R., Quispe, N., Rado, M., Montoya, N., & Velarde, F. (2018). Radar-observed characteristics of precipitation in the tropical high Andes of southern Peru and Bolivia. *Journal of Applied Meteorology and Climatology*, 57, 1441–1458.
- ESA Level-2A algorithm overview [Online]. European Space Agency. <https://sentinels.copernicus.eu/web/sentinel/technical-guides/sentinel-2-msi/level-2a/algorithm-overview> [Accessed 20/06/2023]
- Evaristo, J., Jasechko, S., & McDonnell, J. J. (2015). Global separation of plant transpiration from groundwater and streamflow. *Nature*, 525, 91–94.
- FAO, O. D. L. N. U. P. L. A. Y. L. A. (2022a). Ampliación del área de bofedales para criar alpacas en Chahuanca, Perú. Casos de gestión de turberas.
- FAO, O. D. L. N. U. P. L. A. Y. L. A. (2022b). Restauración hidrológica de bofedales en el Parque Nacional Huascarán. Casos de gestión de turberas.
- Fountain, A. G., & Tangborn, W. V. (1985). The effect of glaciers on streamflow variations. *Water Resources Research*, 21, 579–586.
- Frisbee, M. D., Phillips, F. M., Campbell, A. R., Liu, F., & Sanchez, S. A. (2011). Streamflow generation in a large, alpine watershed in the southern Rocky Mountains of Colorado: Is streamflow generation simply the aggregation of hillslope runoff responses? *Water Resources Research*, 47, W06512.
- Fyffe, C. L., Potter, E., Fugger, S., Orr, A., Fatichi, S., Loarte, E., Medina, K., Hellström, R. Å., Bernat, M., & Aubry-Wake, C. (2021). The energy and mass balance of Peruvian glaciers. *Journal of Geophysical Research: Atmospheres*, 126, e2021JD034911.
- Gat, J. R. (2010). *Isotope hydrology: A study of the water cycle*. World Scientific.
- Gibson, J., & Reid, R. (2010). Stable isotope fingerprint of open-water evaporation losses and effective drainage area fluctuations in a sub-arctic shield watershed. *Journal of Hydrology*, 381, 142–150.
- Glas, R., Lautz, L., Mckenzie, J., Mark, B., Baraer, M., Chavez, D., & Maharaj, L. (2018). A review of the current state of knowledge of

- proglacial hydrogeology in the Cordillera Blanca, Peru. *WIREs Water*, 5, e1299.
- Glas, R., Lautz, L., Mckenzie, J., Moucha, R., Chavez, D., Mark, B., & Lane, J. W. (2019). Hydrogeology of an alpine talus aquifer: Cordillera Blanca, Peru. *Hydrogeology Journal*, 27, 2137–2154.
- Gleeson, T., & Manning, A. H. (2008). Regional groundwater flow in mountainous terrain: Three-dimensional simulations of topographic and hydrogeological controls. *Water Resources Research*, 44, W10403.
- Gordon, R. P., Lautz, L. K., Mckenzie, J. M., Mark, B. G., Chávez, D., & Baraer, M. (2015). Sources and pathways of stream generation in tropical proglacial valleys of the Cordillera Blanca, Peru. *Journal of Hydrology*, 522, 628–644.
- Gröning, M., Lutz, H., Roller-Lutz, Z., Kralik, M., Gourcy, L., & Pölsenstein, L. (2012). A simple rain collector preventing water re-evaporation dedicated for $\delta^{18}\text{O}$ and $\delta^2\text{H}$ analysis of cumulative precipitation samples. *Journal of Hydrology*, 448, 195–200.
- Guy, H., Seimon, A., Perry, L. B., Konecky, B. L., Rado, M., Andrade, M., Potocki, M., & Mayewski, P. A. (2019). Subseasonal variations of stable isotopes in tropical Andean precipitation. *Journal of Hydrometeorology*, 20, 915–933.
- Haiyan, C., Yaning, C., Weihong, L., Xinming, H., Yupeng, L., & Qifei, Z. (2018). Identifying evaporation fractionation and streamflow components based on stable isotopes in the Kaidu River Basin with mountain-oasis system in north-west China. *Hydrological Processes*, 32, 2423–2434.
- Hannah, D. M., Gurnell, A. M., & Mcgregor, G. R. (1999). A methodology for investigation of the seasonal evolution in proglacial hydrograph form. *Hydrological Processes*, 13, 2603–2621.
- Hannah, D. M., Smith, B. P., Gurnell, A. M., & Mcgregor, G. R. (2000). An approach to hydrograph classification. *Hydrological Processes*, 14, 317–338.
- Härer, S., Bernhardt, M., Siebers, M., & Schulz, K. (2018). On the need for a time-and location-dependent estimation of the NDSI threshold value for reducing existing uncertainties in snow cover maps at different scales. *The Cryosphere*, 12, 1629–1642.
- Hayashi, M. (2020). Alpine hydrogeology: The critical role of groundwater in sourcing the headwaters of the world. *Ground Water*, 58, 498–510.
- Hill, A. F., Stallard, R. F., & Rittger, K. (2018). Clarifying regional hydrologic controls of the Marañón River, Peru through rapid assessment to inform system-wide basin planning approaches. *Elementa: Science of the Anthropocene*, 6, 37.
- Hribljan, J., Cooper, D., Sueltenfuss, J., Wolf, E., Heckman, K., Lilleskov, E., & Chimner, R. (2015). Carbon storage and long-term rate of accumulation in high-altitude Andean peatlands of Bolivia.
- IAEA. (2017). Reference sheet for international measurement standards. International Atomic Energy Agency Department Vienna.
- Immerzeel, W. W., Lutz, A. F., Andrade, M., Bahl, A., Biemans, H., Bolch, T., Hyde, S., Brumby, S., Davies, B., & Elmore, A. (2020). Importance and vulnerability of the world's water towers. *Nature*, 577, 364–369.
- INAIGEM, I. N. D. I. E. G. Y. E. D. M. (2023). Inventario Nacional de Glaciares y Lagunas de Origen Glaciar 2023. HUARAZ.
- Irvine-Fynn, T. D., Porter, P. R., Rowan, A. V., Quincey, D. J., Gibson, M. J., Bridge, J. W., Watson, C. S., Hubbard, A., & Glasser, N. F. (2017). Supraglacial ponds regulate runoff from Himalayan debris-covered glaciers. *Geophysical Research Letters*, 44, 11894–11904.
- Isokangas, E., Rossi, P. M., Ronkanen, A.-K., Marttila, H., Rozanski, K., & Kløve, B. (2017). Quantifying spatial groundwater dependence in peatlands through a distributed isotope mass balance approach. *Water Resources Research*, 53, 2524–2541.
- JAXA - Japan Aerospace Exploration Agency. (2021). ALOS World 3D 30 meter DEM. V3.2, Jan 2021. Distributed by OpenTopography. <https://doi.org/10.5069/G94M92HB>
- Jobard, S., & Dzikowski, M. (2006). Evolution of glacial flow and drainage during the ablation season. *Journal of Hydrology*, 330, 663–671.
- King, C., Michelutti, N., Meyer-Jacob, C., Bindler, R., Tapia, P., Grooms, C., & Smol, J. P. (2021). Diatoms and other siliceous indicators track the ontogeny of a “bofedal”(wetland) ecosystem in the Peruvian Andes. *Botany*, 99, 491–505.
- Lahuatue, B., Mosquera, G. M., Páez-Bimos, S., Calispa, M., Vanacker, V., Zapata-Ríos, X., Muñoz, T., & Crespo, P. (2022). Delineation of water flow paths in a tropical Andean headwater catchment with deep soils and permeable bedrock. *Hydrological Processes*, 36, e14725.
- Landwehr, J., & Coplen, T. (2006). Line-conditioned excess: A new method for characterizing stable hydrogen and oxygen isotope ratios in hydrologic systems. In *International conference on isotopes in environmental studies* (pp. 132–135). IAEA.
- Lee, J., Feng, X., Faiia, A. M., Posmentier, E. S., Kirchner, J. W., Osterhuber, R., & Taylor, S. (2010). Isotopic evolution of a seasonal snowcover and its melt by isotopic exchange between liquid water and ice. *Chemical Geology*, 270, 126–134.
- Leibowitz, S. G., Mushet, D. M., & Newton, W. E. (2016). Intermittent surface water connectivity: Fill and spill vs. fill and merge dynamics. *Wetlands*, 36, 323–342.
- MacDonald, A. M., Black, A. R., Ó Dochartaigh, B. É., Everest, J., Darling, W. G., Flett, V., & Peach, D. W. (2016). Using stable isotopes and continuous meltwater river monitoring to investigate the hydrology of a rapidly retreating Icelandic outlet glacier. *Annals of Glaciology*, 57, 151–158.
- Mackay, J. D., Barrand, N. E., Hannah, D. M., Krause, S., Jackson, C. R., Everest, J., MacDonald, A. M., & Ó Dochartaigh, B. É. (2020). Proglacial groundwater storage dynamics under climate change and glacier retreat. *Hydrological Processes*, 34, 5456–5473.
- Mackay, J. D., Barrand, N. E., Hannah, D. M., Potter, E., Montoya, N., & Buytaert, W. (2024). Physically-based modelling of glacier evolution under climate change in the tropical Andes. *EGU sphere*, 2024, 1–37.
- Maldonado Fonkén, M. (2014). An introduction to the bofedales of the Peruvian High Andes. *Mires and Peat*, 15, 1–13.
- Mayernik, C. M., Ewing, S. A., Sigler, W. A., Jencso, K. G., & Payn, R. A. (2024). Water isotopic composition traces source and dynamics of water supply in a semi-arid agricultural landscape. *Hydrological Processes*, 38, e15069.
- Mcclymont, A. F., Hayashi, M., Bentley, L. R., Muir, D., & Ernst, E. (2010). Groundwater flow and storage within an alpine meadow-talus complex. *Hydrology and Earth System Sciences*, 14, 859–872.
- Mosquera, G. M., Céleri, R., Lazo, P. X., Vaché, K. B., Perakis, S. S., & Crespo, P. (2016). Combined use of isotopic and hydrometric data to conceptualize ecohydrological processes in a high-elevation tropical ecosystem. *Hydrological Processes*, 30, 2930–2947.
- Muir, D. L., Hayashi, M., & Mcclymont, A. F. (2011). Hydrological storage and transmission characteristics of an alpine talus. *Hydrological Processes*, 25, 2954–2966.
- NASA. (2013). Shuttle Radar Topography Mission Global 1 arc second. In: Center, N. E. L. P. D. A. A. (ed.).
- Noor, K., Marttila, H., Kløve, B., Welker, J. M., & Ala-Aho, P. (2023). The spatiotemporal variability of snowpack and snowmelt water ^{18}O and ^2H isotopes in a subarctic catchment. *Water Resources Research*, 59, e2022WR033101.
- Ó Dochartaigh, B., Archer, N., Peskett, L., MacDonald, A. M., Black, A., Auton, C., Merritt, J., Goody, D., & Bonell, M. (2019). Geological structure as a control on floodplain groundwater dynamics. *Hydrogeology Journal*, 27, 703–716.
- Ó Dochartaigh, B. É., MacDonald, A. M., Black, A. R., Everest, J., Wilson, P., Darling, W. G., Jones, L., & Raines, M. (2019). Groundwater–glacier meltwater interaction in proglacial aquifers. *Hydrology and Earth System Sciences*, 23, 4527–4539.
- Ohlanders, N., Rodriguez, M., & Mcphee, J. (2013). Stable water isotope variation in a Central Andean watershed dominated by glacier and snowmelt. *Hydrology and Earth System Sciences*, 17, 1035–1050.

- Oyague, E., & Cooper, D. J. (2020). Peatlands of the central Andes puna, South America. *Wetland Science & Practice*, 37, 255–260.
- Oyague, E., Cooper, D. J., & Ingol, E. (2022). Effects of land use on the hydrologic regime, vegetation, and hydraulic conductivity of peatlands in the central Peruvian Andes. *Journal of Hydrology*, 609, 127687.
- Penn, K., Marshall, S. J., & Sinclair, K. E. (2023). Seasonal enrichment of heavy isotopes in meltwater runoff from Haig Glacier, Canadian Rocky Mountains. *Frontiers in Earth Science*, 11, 1125877.
- Penna, D., Engel, M., Bertoldi, G., & Comiti, F. (2017). Towards a tracer-based conceptualization of meltwater dynamics and streamflow response in a glacierized catchment. *Hydrology and Earth System Sciences*, 21, 23–41.
- Perez, N., & Loisel, J. (2023). Synthesis of high-Andean peat cores reveals suite of Holocene climate conditions favorable for peat formation. *Quaternary Science Reviews*, 322, 108413.
- Perry, L. B., Seimon, A., Andrade-Flores, M. F., Endries, J. L., Yuter, S. E., Velarde, F., Arias, S., Bonshoms, M., Burton, E. J., & Winkelmann, I. R. (2017). Characteristics of precipitating storms in glacierized tropical Andean cordilleras of Peru and Bolivia. *Annals of the American Association of Geographers*, 107, 309–322.
- Perry, L. B., Seimon, A., & Kelly, G. M. (2014). Precipitation delivery in the tropical high Andes of southern Peru: New findings and paleoclimatic implications. *International Journal of Climatology*, 34, 197–215.
- Pesántez, J., Birkel, C., Mosquera, G. M., Célleri, R., Contreras, P., Cárdenas, I., & Crespo, P. (2023). Bridging the gap from hydrological to biogeochemical processes using tracer-aided hydrological models in a tropical montane ecosystem. *Journal of Hydrology*, 619, 129328.
- Polk, M. H., Young, K. R., Baraer, M., Mark, B. G., Mckenzie, J. M., Bury, J., & Carey, M. (2017). Exploring hydrologic connections between tropical mountain wetlands and glacier recession in Peru's Cordillera Blanca. *Applied Geography*, 78, 94–103.
- Postigo, J. C. (2021). The role of social institutions in indigenous Andean Pastoralists' adaptation to climate-related water hazards. *Climate and Development*, 13, 780–791.
- Rezanezhad, F., Price, J. S., Quinton, W. L., Lennartz, B., Milojevic, T., & Van Cappellen, P. (2016). Structure of peat soils and implications for water storage, flow and solute transport: A review update for geochemists. *Chemical Geology*, 429, 75–84.
- Ross, A. C., Mendoza, M. M., Drenkhan, F., Montoya, N., Baiker, J. R., Mackay, J. D., Hannah, D. M., & Buytaert, W. (2023). Seasonal water storage and release dynamics of bofedal wetlands in the Central Andes. *Hydrological Processes*, 37, e14940.
- Salzmann, N., Huggel, C., Rohrer, M., Silverio, W., Mark, B. G., Burns, P., & Portocarrero, C. (2013). Glacier changes and climate trends derived from multiple sources in the data scarce Cordillera Vilcanota region, southern Peruvian Andes. *The Cryosphere*, 7, 103–118.
- Sánchez-Murillo, R., Durán-Quesada, A. M., Esquivel-Hernández, G., Rojas-Cantillano, D., Birkel, C., Welsh, K., Sánchez-Llull, M., Alonso-Hernández, C. M., Tetzlaff, D., Soulsby, C., Boll, J., Kurita, N., & Cobb, K. M. (2019). Deciphering key processes controlling rainfall isotopic variability during extreme tropical cyclones. *Nature Communications*, 10, 4321.
- Soberon, D., Rodriguez, R., Choquehuanca, S., & Gomez, W. (2022). Geología del cuadrángulo de Corani (hojas 28u1, 28u2, 28u3, 28u4). Actualización Carta Geológica Nacional (Escala 1:50 000). Lima, Peru: INGEMMET.
- Somers, L. D., Gordon, R. P., Mckenzie, J. M., Lautz, L. K., Wigmore, O., Glose, A., Glas, R., Aubry-Wake, C., Mark, B., Baraer, M., & Condom, T. (2016). Quantifying groundwater–surface water interactions in a proglacial valley, Cordillera Blanca, Peru. *Hydrological Processes*, 30, 2915–2929.
- Somers, L. D., & Mckenzie, J. M. (2020). A review of groundwater in high mountain environments. *WIREs Water*, 7, e1475.
- Somers, L. D., Mckenzie, J. M., Mark, B. G., Lagos, P., Ng, G.-H. C., Wickert, A. D., Yarleque, C., Baraer, M., & Silva, Y. (2019). Groundwater buffers decreasing glacier melt in an Andean watershed—but not forever. *Geophysical Research Letters*, 46, 13016–13026.
- Soulsby, C., Scheliga, B., Neill, A., Comte, J. C., & Tetzlaff, D. (2021). A longer-term perspective on soil moisture, groundwater and stream flow response to the 2018 drought in an experimental catchment in the Scottish highlands. *Hydrological Processes*, 35, e14206.
- Sprenger, M., Leistert, H., Gimbel, K., & Weiler, M. (2016). Illuminating hydrological processes at the soil-vegetation-atmosphere interface with water stable isotopes. *Reviews of Geophysics*, 54, 674–704.
- Sprenger, M., Tetzlaff, D., Tunaley, C., Dick, J., & Soulsby, C. (2017). Evaporation fractionation in a peatland drainage network affects stream water isotope composition. *Water Resources Research*, 53, 851–866.
- St Amour, N. A., Gibson, J. J., Edwards, T. W., Prowse, T. D., & Pietroniro, A. (2005). Isotopic time-series partitioning of streamflow components in wetland-dominated catchments, lower Liard River basin, Northwest Territories, Canada. *Hydrological Processes: An International Journal*, 19, 3357–3381.
- Stichler, W., Schotterer, U., Fröhlich, K., Ginot, P., Kull, C., Gäggeler, H., & Pouyaud, B. (2001). Influence of sublimation on stable isotope records recovered from high-altitude glaciers in the tropical Andes. *Journal of Geophysical Research: Atmospheres*, 106, 22613–22620.
- Suarez, W., Macedo, N., Montoya, N., Arias, S., Schauwecker, S., Huggel, C., Rohrer, M., & Condom, T. (2015). Balance energético neto (2012–2014) y evolución temporal del nevado Quisoquipina en la región de Cusco (1990–2010). *Revista Peruana Geo-Atmosférica*, 4, 80–92.
- Swift, D. A., Nienow, P. W., Hoey, T. B., & Mair, D. W. (2005). Seasonal evolution of runoff from Haut Glacier d'Arolla, Switzerland and implications for glacial geomorphic processes. *Journal of Hydrology*, 309, 133–148.
- Taylor, L. S., Quincey, D. J., Smith, M. W., Potter, E. R., Castro, J., & Fyffe, C. L. (2022). Multi-decadal glacier area and mass balance change in the Southern Peruvian Andes. *Frontiers in Earth Science*, 10, 1–14.
- Taylor, S., Feng, X., Kirchner, J. W., Osterhuber, R., Klaue, B., & Renshaw, C. E. (2001). Isotopic evolution of a seasonal snowpack and its melt. *Water Resources Research*, 37, 759–769.
- Terzer-Wassmuth, S., Ortega, L., Araguás-Araguás, L., & Wassenaar, L. I. (2020). The first IAEA inter-laboratory comparison exercise in Latin America and the Caribbean for stable isotope analyses of water samples. *Isotopes in Environmental and Health Studies*, 56, 391–401.
- Thompson, L. G., Mosley-Thompson, E., Bolzan, J. F., & Koci, B. R. (1985). A 1500-year record of tropical precipitation in ice cores from the Quelccaya ice cap, Peru. *Science*, 229, 971–973.
- Valdivielso, S., Vázquez-Suñé, E., & Custodio, E. (2020). Origin and variability of oxygen and hydrogen isotopic composition of precipitation in the Central Andes: A review. *Journal of Hydrology*, 587, 124899.
- Valois, R., Araya Vargas, J., Macdonell, S., Guzmán Pinones, C., Fernandoy, F., Yáñez Carrizo, G., Cuevas, J. G., Sproles, E. A., & Maldonado, A. (2021). Improving the underground structural characterization and hydrological functioning of an Andean peatland using geoelectrics and water stable isotopes in semi-arid Chile. *Environmental Earth Sciences*, 80, 1–14.
- Van Der Kamp, G., & Hayashi, M. (2009). Groundwater-wetland ecosystem interaction in the semiarid glaciated plains of North America. *Hydrogeology Journal*, 17, 203–214.
- Van Tiel, M., Kohn, I., Van Loon, A. F., & Stahl, K. (2020). The compensating effect of glaciers: Characterizing the relation between interannual streamflow variability and glacier cover. *Hydrological Processes*, 34, 553–568.
- Viviroli, D., Dürr, H. H., Messerli, B., Meybeck, M., & Weingartner, R. (2007). Mountains of the world, water towers for humanity: Typology, mapping, and global significance. *Water Resources Research*, 43, W07447.

- Viviroli, D., Kummu, M., Meybeck, M., Kallio, M., & Wada, Y. (2020). Increasing dependence of lowland populations on mountain water resources. *Nature Sustainability*, 3, 917–928.
- Vuille, M., Carey, M., Huggel, C., Buytaert, W., Rabatel, A., Jacobsen, D., Soruco, A., Villacis, M., Yarleque, C., & Timm, O. E. (2018). Rapid decline of snow and ice in the tropical Andes—Impacts, uncertainties and challenges ahead. *Earth-Science Reviews*, 176, 195–213.
- Vyse, S. A., Taie Semiromi, M., Lischeid, G., & Merz, C. (2020). Characterizing hydrological processes within kettle holes using stable water isotopes in the Uckermark of northern Brandenburg, Germany. *Hydrological Processes*, 34, 1868–1887.
- Williams, M. W., Hood, E. W., Ostberg, G., Francou, B., & Galarraga, R. (2001). Synoptic survey of surface water isotopes and nutrient concentrations, Páramo high-elevation region, Antisana Ecological Reserve, Ecuador. *Arctic, Antarctic, and Alpine Research*, 33, 397–403.
- Wunderlich, W., Lang, M., Keating, K., Perez, W. B., & Oshun, J. (2023). The role of peat-forming bofedales in sustaining baseflow in the humid puna. *Journal of Hydrology: Regional Studies*, 47, 101394.
- Yager, K., Valdivia, C., Slayback, D., Jimenez, E., Meneses, R. I., Palabral, A., Bracho, M., Romero, D., Hubbard, A., & Pacheco, P. (2019). Socio-ecological dimensions of Andean pastoral landscape change: Bridging

traditional ecological knowledge and satellite image analysis in Sajama National Park, Bolivia. *Regional Environmental Change*, 19, 1353–1369.

Zhou, S., Wang, Z., & Joswiak, D. R. (2014). From precipitation to runoff: Stable isotopic fractionation effect of glacier melting on a catchment scale. *Hydrological Processes*, 28, 3341–3349.

SUPPORTING INFORMATION

Additional supporting information can be found online in the Supporting Information section at the end of this article.

How to cite this article: Gribbin, T., Mackay, J. D., MacDonald, A., Hannah, D. M., Buytaert, W., Baiker, J. R., Montoya, N., Perry, L. B., Seimon, A., Rado, M., Arias, S., & Vargas, M. (2024). Bofedal wetland and glacial melt contributions to dry season streamflow in a high-Andean headwater watershed. *Hydrological Processes*, 38(8), e15237. <https://doi.org/10.1002/hyp.15237>